

Control of Inhibitory Synaptic Outputs by Low Excitability of Axon Terminals Revealed by Direct Recording

Highlights

- Cultured Purkinje cell (PC) axon terminals contain a large RRP of synaptic vesicles
- Release probability of RRP vesicles is extremely low in cultured PC axon terminals
- Action potentials that conduct reliably along the axon are attenuated close to terminals
- Attenuated action potentials control short-term synaptic depression

Authors

Shin-ya Kawaguchi, Takeshi Sakaba

Correspondence

skawaguc@mail.doshisha.ac.jp (S.-y.K.),
tsakaba@mail.doshisha.ac.jp (T.S.)

In Brief

By directly recording from the axon and terminal of a cultured cerebellar Purkinje cell, Kawaguchi and Sakaba demonstrate that action potential amplitudes are attenuated around axon terminals upon high-frequency activation, leading to short-term depression.



Control of Inhibitory Synaptic Outputs by Low Excitability of Axon Terminals Revealed by Direct Recording

Shin-ya Kawaguchi^{1,*} and Takeshi Sakaba^{1,*}

¹Graduate School of Brain Science, Doshisha University, Kizugawa-Shi, Kyoto, 619-0225, Japan

*Correspondence: skawaguc@mail.doshisha.ac.jp (S.-y.K.), tsakaba@mail.doshisha.ac.jp (T.S.)

<http://dx.doi.org/10.1016/j.neuron.2015.02.013>

SUMMARY

An axon is thought to faithfully conduct action potentials to its terminals. However, many features of the axon and axon terminals, especially at inhibitory synapses, remain unknown. By directly recording from the axon and terminal of a cultured cerebellar Purkinje cell (PC), we demonstrate that low membrane excitability of axon terminals shapes synaptic output. Simultaneous measurements of presynaptic capacitance and evoked IPSCs revealed PC axon terminals contained large readily releasable synaptic vesicles that exhibited a low release probability. Nevertheless, IPSCs evoked by stimulating a PC soma underwent frequency-dependent depression. Direct axonal recordings showed that high-frequency action potentials were faithfully conducted over axonal bifurcations but were attenuated around terminals. Sparse Na⁺ channels relative to enriched voltage-gated K⁺ channels in terminals caused short-term depression of IPSCs by reducing Ca²⁺ influx. Together with confirmation in slice recordings, our findings reveal a presynaptic mechanism that shapes short-term synaptic depression without depleting releasable vesicles.

INTRODUCTION

Efficacy and activity-dependent plasticity of synaptic transmission impact computations of the nervous system. Short-term synaptic plasticity lasts over periods of milliseconds or minutes and is crucial for information processing (Abbott and Regehr, 2004). At many central synapses, frequent and repetitive activity leads to a decrease in synaptic strength, termed short-term synaptic depression. At glutamatergic synapses, depletion of the readily releasable pool (RRP) of synaptic vesicles is considered to be one of the major mechanisms underlying such synaptic depression (Zucker and Regehr, 2002; Fioravante and Regehr, 2011). Other mechanisms at presynaptic varicosities include inactivation of release sites (Neher and Sakaba, 2008; Pan and Zucker, 2009), Ca²⁺ current inactivation, and action potential (AP) conduction failure at axonal branches (Xu and Wu, 2005;

Catterall and Few, 2008; Brody and Yue, 2000; Prakriya and Mennerick, 2000). In addition, postsynaptic mechanisms such as receptor desensitization shape synaptic depression (Zucker and Regehr, 2002). Many types of inhibitory synapses also exhibit short-term depression (Vincent and Marty, 1996; Galarreta and Hestrin, 1998; Kraushaar and Jonas, 2000; Sakaba, 2008). However, compared to excitatory synapses, the mechanisms of short-term plasticity remain largely unknown at inhibitory synapses, despite their functional importance (Lawrence and McBain, 2003; Jonas et al., 2004). One possible mechanism is the activity-dependent depletion of the RRP (Moulder and Mennerick, 2005), as reported for excitatory synapses. In addition, unidentified mechanisms upstream of exocytosis (release-independent component of depression) or the properties associated with neurotransmitter release may be responsible (Kraushaar and Jonas, 2000; Hefft et al., 2002; Kirischuk et al., 2002; but see Volynski et al., 2006).

To clarify the mechanism of frequency-dependent modulation of inhibitory synaptic output, it is necessary to directly record from presynaptic boutons. However, the small size of presynaptic terminals has hindered their direct functional analysis, with the exception of a few large presynaptic structures (Borst et al., 1995; Geiger and Jonas, 2000; Southan and Robertson, 1998) and synaptosomes (Smith et al., 2004, but see a recent study by Novak et al., 2013). In addition, technical challenges have hampered the study of information transmission from the axon to its terminals. Specific questions remain concerning whether the transmission is faithful or plastic and how it might affect synaptic transmission and/or plasticity (Debanne, 2004). To address such questions, we performed direct patch-clamp recordings from the axon and/or axon terminals of cultured Purkinje cells (PCs). These neurons form synapses similar to that observed in intact preparations (Hirano and Kasono, 1993), allowing for simultaneous recording of the postsynaptic response. From such recordings, we were able to examine the electrical properties of axons and terminals as well as the relatively unknown properties of transmitter release at inhibitory synapses.

PCs are the sole output neurons of the cerebellar cortex, and they potently inhibit neurons in the deep cerebellar nuclei (DCN). PC axons are relatively thick and can faithfully transmit sodium APs up to over 200 Hz (Khaliq and Raman, 2005; Monsivais et al., 2005). Synaptic transmission at PC-DCN neuron synapses exhibit short-term depression upon repetitive stimulation in a manner dependent on stimulation frequency (Telgkamp and

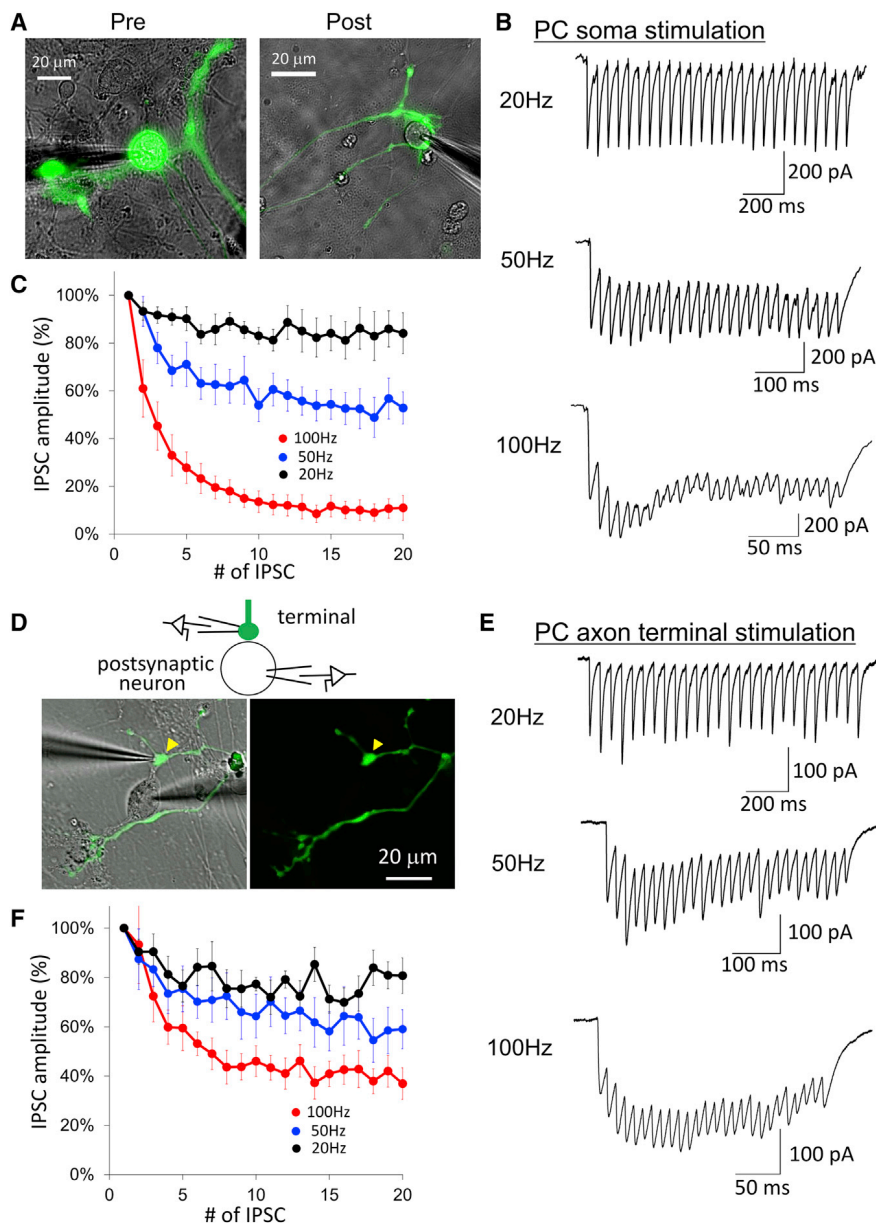


Figure 1. Frequency-Dependent Depression of PC Outputs

(A) Images of a synaptically connected EGFP-labeled PC (left) and postsynaptic neuron (right). Whole-cell recordings were performed from both. (B) Representative traces of IPSCs elicited by train stimulation at 20, 50, and 100 Hz. Each trace was the average of 20 traces. (C) Peak IPSC amplitudes normalized to the first IPSC amplitude; $n = 7$ pairs for each. (D) Images of a paired patch-clamp recording from an EGFP-expressing PC axon terminal (yellow arrowhead) and postsynaptic cell. (E) Representative average traces of IPSCs evoked by current injection directly into a presynaptic terminal at 20, 50, and 100 Hz. (F) Peak amplitudes of IPSCs caused by direct activation of the presynaptic terminal were normalized to the first IPSC amplitude; $n = 7$ pairs for each. Data are presented as mean \pm SEM. See also Figure S1.

RESULTS

Frequency-Dependent Depression of PC Outputs

We first performed paired recordings from a PC and a target neuron in culture. To visualize the axons of PCs specifically, EGFP was expressed using an adeno-associated virus (AAV) vector that preferentially infected PCs in the cerebellum (Kaneko et al., 2011) (Figure 1A). Each PC had an extended axon with many bifurcations, which tended to form synapses onto a particular cell type in the DCN (Figures 1A and S1; see Supplemental Experimental Procedures). PCs were voltage clamped at -70 mV and the paired target neuron clamped at voltages between -50 and -100 mV. APs were elicited at 20, 50, or 100 Hz in the PC soma, and the resulting evoked IPSCs in the target cell exhibited a frequency-

dependent depression (20 Hz, $84\% \pm 6\%$, average of 16th–20th IPSCs, 50 Hz, $53\% \pm 7\%$, 100 Hz, $10\% \pm 4\%$, $n = 7$ pairs) (Figures 1B and 1C). This was in agreement with previous studies conducted at PC-DCN synapses in slice (Telgkamp and Raman, 2002; Pedroarena and Schwarz, 2003).

To examine mechanisms of the frequency-dependent depression of PC outputs, we used the EGFP fluorescence as a guide to directly patch-clamp a PC axon terminal, which usually ranged in size from 1 to 3 μm . Although technically demanding, the success of this method was due largely to the visibility and high accessibility of boutons in the culture preparation (Figure 1D). IPSCs were elicited by direct activation of the presynaptic terminal following either a depolarizing pulse (0 mV for 1 to 2 ms) or current injection (400–1,000 pA for 1 to 2 ms) (Figure 1E). The resulting IPSC was similar in amplitude and time course to the

Raman, 2002; Pedroarena and Schwarz, 2003; Telgkamp et al., 2004), although the underlying mechanisms are unknown. We have taken advantage of a cultured PC expressing enhanced green fluorescent protein (EGFP) to directly visualize its axon and presynaptic varicosities and have performed direct recordings from the axon and its terminal. Paired recordings of presynaptic membrane capacitance (C_m) and postsynaptic currents demonstrated that PC axon terminals, in spite of undergoing frequency-dependent depression, contain a large number of RRP vesicles and a very low release probability. Therefore, vesicle pool depletion cannot account for short-term depression at this synapse. Instead, AP conduction to the axon terminals is negatively regulated by the low membrane excitability of boutons in an activity-dependent manner, leading to short-term synaptic depression.

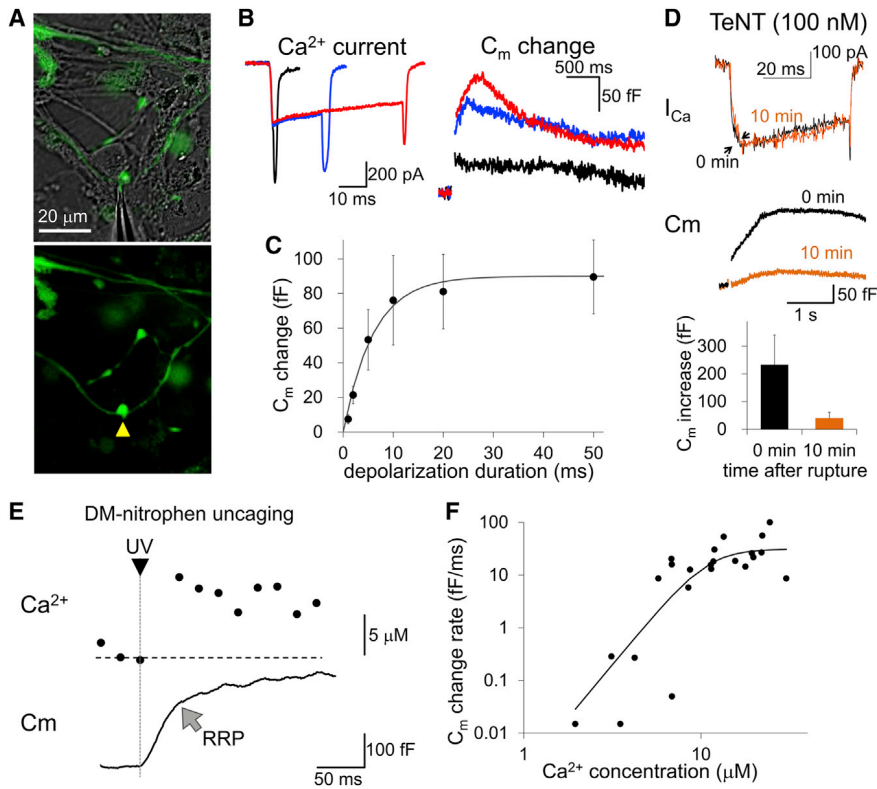


Figure 2. Cm Increase by Direct Depolarization or Ca²⁺ Uncaging in a PC Axon Terminal (A) Images of a presynaptic terminal recorded in the whole-cell patch-clamp configuration.

(B) Representative traces of presynaptic Ca²⁺ currents and the resultant change in Cm caused by 2 (black), 20 (blue), and 50 ms (red) depolarizing pulses.

(C) Amplitudes of Cm changes (mean ± SEM, 200 ms after the end of the Ca²⁺ current) were plotted against depolarization pulse duration; n = 9. (D) Top: Presynaptic Ca²⁺ currents and Cm change upon a 50 ms depolarization pulse immediately or 10 min after the start of whole-cell recording with 100 nM TeNT included in the patch pipette. Bottom: Averaged Cm changes immediately or 10 min after the TeNT application; n = 4 cells.

(E) Representative time courses of [Ca²⁺]_i and Cm increase caused by UV-mediated Ca²⁺ uncaging. Sharp Cm increase corresponds to the RRP, and the subsequent gradual increase presumably corresponds to the release of replenished vesicles.

(F) The peak rate of Cm increase was plotted against [Ca²⁺]_i. Hill equation curve (K_{Ca²⁺} of 11 μM and Hill coefficient of 4.04) obtained by fitting the data with the least square method is shown by the black line.

IPSC triggered by a spontaneous AP (see Figure S1). Surprisingly, when IPSC trains were triggered by repetitive direct stimulation of a presynaptic varicosity, the depression of IPSC amplitude by 100 Hz stimulation was markedly reduced compared to somatic stimulation (20 Hz, 81% ± 7%, average of 16th–20th IPSCs, $p = 0.54$ by Student's *t* test, compared with soma stimulation; 50 Hz, 60% ± 9%, $p = 0.53$; 100 Hz, 40% ± 6%, $p = 0.001$, $n = 7$ pairs) (Figure 1F). Thus, a large part of the high-frequency-dependent depression at PC-DCN synapses is presynaptic in origin. However, the depression might be due not to the release mechanisms such as depletion of the releasable vesicles pool, but to the activity-dependent changes at the axon or terminals, such as altered presynaptic Ca²⁺ influx, conduction failure, or attenuation of APs.

Characterization of the RRP, Release Probability, and Intracellular Ca²⁺ Sensitivity of Transmitter Release at a PC Terminal

To examine the kinetics of transmitter release from a PC terminal, we measured Cm of a presynaptic varicosity under the whole-cell configuration (Neher and Marty, 1982) before and after (~200 ms, average period of 100 ms) the depolarization pulse (Figure 2A). TTX (1 μM) and TEA (2 mM) were applied to the external solution to block Na⁺ and K⁺ channels, respectively. In addition, Cs-based intracellular solution was used to isolate presynaptic Ca²⁺ currents. To limit the Cm change to single presynaptic terminal, we recorded from a bouton with few neighboring varicosities (Figure 2A). Considering experimental conditions (space-clamp of the terminal and neighboring axonal regions),

Cm changes likely reflect exocytosis and endocytosis of vesicles at the patch-clamped terminal (see Supplemental Experimental Procedures). The duration of the depolarization pulse was altered to change the duration of Ca²⁺ influx (Figure 2B). We found that the Cm of PC terminals increased depending on the duration of the depolarization pulse (2 ms, 21 ± 5 fF; 10 ms, 76 ± 26 fF; 50 ms, 90 ± 21 fF) (Figures 2B and 2C). For longer pulses, a continuous increase in Cm was observed lasting for approximately 1 s after the depolarization ceased, probably reflecting asynchronous release. When SNARE complex function for vesicle exocytosis was inhibited by VAMP2 cleavage by applying tetanus toxin (TeNT, 100 nM) into the terminal through a patch pipette, the Cm increase was suppressed by about 80%–90% within 10 min after whole-cell rupture (15% ± 4%, $p = 0.0002$, paired *t* test) (Figure 2D). Therefore, the increase in Cm mostly reflected exocytosis of synaptic vesicles. In Figure 2C, the time course of Cm increase could be fitted by a single exponential with a time constant of 6 ms and a maximal amplitude of 90 fF, though the latter was variable (ranging from 30 fF to 250 fF). The maximal amplitude corresponds to the RRP of synaptic vesicles. Assuming the Cm of a single synaptic vesicle is 65 aF (estimated from the value of Figure 3F), on average, about 1,000–1,500 synaptic vesicles were released in response to a single 10 ms depolarization pulse. Thus, the RRP size is very large in a cultured PC terminal. Increasing the intracellular EGTA concentration from 0.5 to 5 mM altered neither the time course nor maximal amplitude of Cm ($n = 4$ cells, time constant = 6 ms and a maximal amplitude of 110 fF; data not shown), in agreement with other inhibitory synapses where transmitter

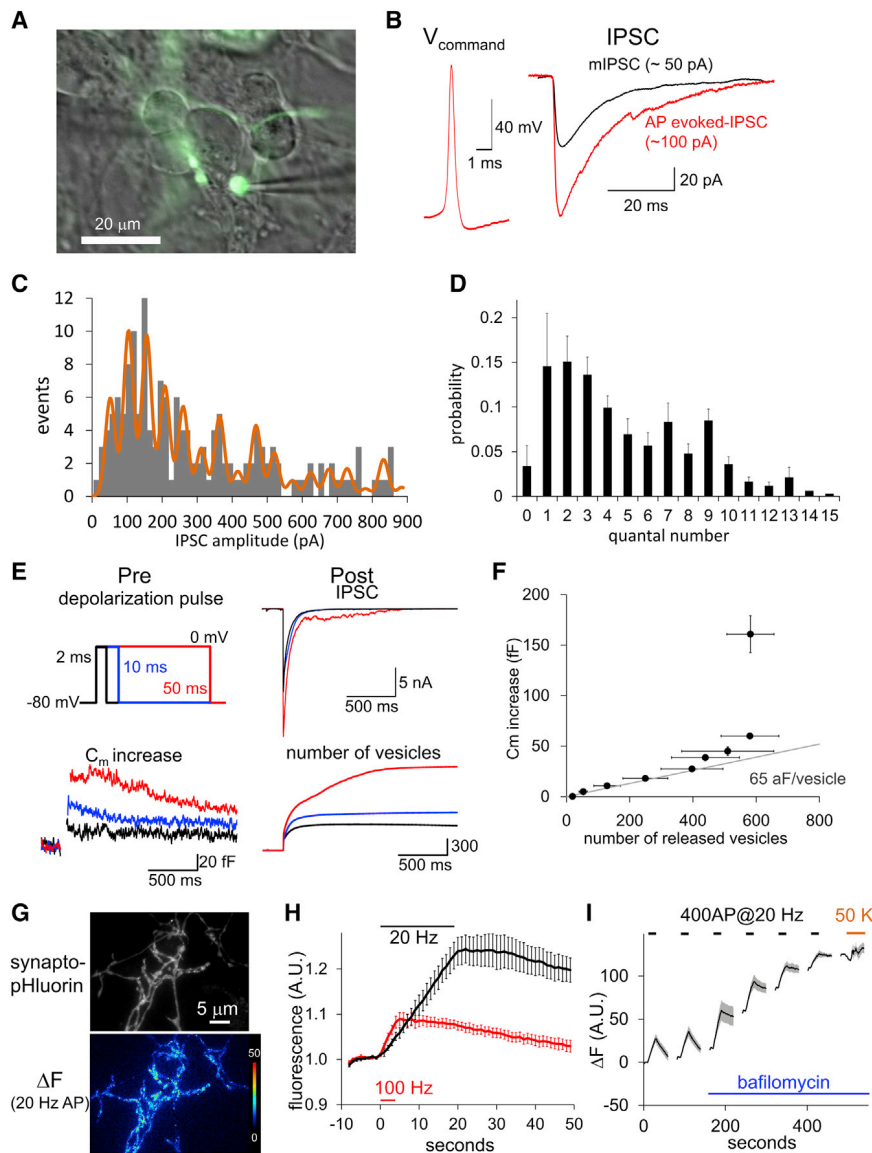


Figure 3. Paired Recordings of Presynaptic Exocytosis and IPSCs

(A) Image of a dual recording from a presynaptic terminal and a connected postsynaptic neuron. (B) Presynaptic AP-like voltage command and the corresponding evoked IPSC (average of 42 traces, red). For comparison, the mIPSC trace (average of 217 traces) recorded from the same cell is overlaid. (C) IPSC amplitude distribution histogram with approximately ten apparent discrete steps recorded from a paired recording as shown in (A). The orange distribution shows fitting of the IPSC distribution with a combination of single Gaussian distributions exhibiting a mean and SD of 60 and 15 pA, respectively. (D) Distribution of quantal number averaged from six pairs. (E) Time course of the presynaptic Cm increase, resulting IPSC, and cumulative number of released vesicles estimated by deconvolution, in response to different durations of terminal depolarization. (F) The Cm increase was plotted against total released vesicles estimated by deconvolution. Data were obtained from ten synapses. The Cm increase showed a linear relation to the number of released vesicles for <math>< 400</math> released vesicles (gray line). (G) Fluorescent images of synaptotHluorin expressed in a PC. The lower panel shows the increase in fluorescence during a 20 Hz AP train stimulation. (H) Normalized time courses of synaptotHluorin fluorescence intensity over time following 400 APs at 100 (red) or 20 Hz (black); $n = 40$ terminals from eight cells. (I) Time course of fluorescence increase during rounds of AP train stimulation (400 APs at 20 Hz) before and after bafilomycin application (indicated by blue bar). To confirm that the majority of releasable vesicles were depleted, 50 mM K^+ -containing solution was applied at the end of the recording; $n = 25$ terminals from five cells. Data are presented as mean \pm SEM. See also Figure S2.

release was found to be EGTA insensitive (Bucurenciu et al., 2008). On the other hand, loading 5 mM of the relatively fast Ca^{2+} chelator BAPTA (with a similar K_d to EGTA) into the PC axon terminal reduced the Cm increase by about 80% (Cm maximally increased by 19 ± 11 fF with a time constant of 9 ms, $n = 5$ cells). It should be noted that the amplitude of Cm increase was substantially smaller in PC terminals of slice preparation at P9–P16 (see Figure S6A), suggesting that the RRP size of small axon terminals in intact preparation at young developmental age is much smaller.

In order to examine the release mechanism quantitatively, we next applied the Ca^{2+} uncaging method to the PC terminal (Delaney and Zucker, 1990; Heidelberger et al., 1994). The caged Ca^{2+} compound DM-Nitrophen (2–5 mM) and the Ca^{2+} indicator Fura2-FF (200 μ M) were applied to the terminal via the patch pipette. Flash photolysis of DM-Nitrophen uniformly elevated the intra-terminal Ca^{2+} concentration ($[Ca^{2+}]_i$) (Fig-

ure 2E), which caused a linear increase in Cm when $[Ca^{2+}]_i$ was low. When the $[Ca^{2+}]_i$ was high, the Cm showed a sharp increase (Figure 2E), which peaked at an average of 80 ± 20 fF ($n = 10$ terminals). The maximal Cm increase reflects the RRP size, and the value attained was similar to that elicited by a depolarizing pulse (see above, Figure 2C), suggesting a homogenous pool of vesicles. As illustrated in Figure 2E, the Cm showed a slow increase following the initial phase, presumably reflecting vesicle replenishment. As a result, the entire time course could be fitted by the sum of an exponential and a linear function. By changing the $[Ca^{2+}]_i$ in the terminal, we have also measured the intracellular Ca^{2+} sensitivity for transmitter release. When plotted as a function of $[Ca^{2+}]_i$, the release rate showed an approximate 4th power dependency and the $[Ca^{2+}]_i$ required for half-maximal activation of release was approximately 11 μ M (Figure 2F). The relationship was similar to that observed for the calyx of Held and cerebellar basket

cell (BC) terminals (Bollmann et al., 2000; Schneggenburger and Neher, 2000; Sakaba, 2008).

To further examine the size of the RRP and release probability (Pr), we performed simultaneous recordings of presynaptic Cm and IPSCs (Figure 3A). Presynaptic terminals were voltage clamped with a Cs-based internal solution in the presence of TTX and TEA, stimulated with an AP voltage waveform previously recorded from another terminal. As shown in Figure 3B, the amplitude of evoked IPSCs recorded from the postsynaptic neuron was only about twice that of miniature IPSCs (mIPSCs), which presumably corresponded to the synaptic response caused by single vesicle release. Thus, several vesicles (4.8 ± 1.7 , $n = 8$ pairs) are released at a single synapse in response to a single AP. Representative IPSCs recorded from a pair showed approximately ten discrete steps in response to the AP-like voltage command (Figure 3C; also see Figure S2). The distribution of IPSC amplitudes could be fitted by combinations of quantal IPSC amplitude distributions with multiple integer amplitudes. The quantal distribution obtained from six pairs suggested that, on average, 4.8 ± 0.5 quanta are released from a single AP (Figure 3D).

Our findings that cultured PC terminals have a low Pr and a large RRP were supported by the following experiments. Prolonged square depolarization pulses (to 0 mV) produced a >100-fold increase in both vesicle fusion events and IPSC amplitude (Figure 3E). The total number of released synaptic vesicles, estimated by deconvolution of each IPSC trace with the mIPSC trace (Sakaba, 2008), showed a linear relationship to the measured Cm jump, with an initial slope of 65 aF/vesicle (Figure 3F). This value is toward the higher end of the range (30–85 aF) estimated from a synaptic vesicle with a size of 35–50 nm in PC terminals (Takei et al., 1992), as well as values calculated from on-cell capacitance measurements (He et al., 2006). It is possible that the number of released vesicles even following limited exocytosis might be underestimated in deconvolution analysis due to high receptor occupancy at GABAergic synapses (Auger and Marty, 2000). We also note that the relationship between Cm and the estimated number of vesicles has some variability. For large amounts of exocytosis (>400 vesicles), the slope steeply increased, indicating that postsynaptic responses did not follow linearly to vesicle release. This is most likely because of strong postsynaptic receptor saturation and/or desensitization (Telgkamp et al., 2004; Pugh and Raman, 2005). Nevertheless, the postsynaptic recordings confirmed a large RRP (at least >500 vesicles). Taken together, the simultaneous recordings of presynaptic Cm and IPSCs at a single synapse revealed thousands of RRP vesicles that have an extremely low (~ 0.003) release probability in response to a single AP.

From the relationship between $[Ca^{2+}]_i$ and release rates (Figure 2F), we estimated the $[Ca^{2+}]_i$ during an AP at the transmitter release site using the five-step release model (Bollmann et al., 2000; Schneggenburger and Neher, 2000). The peak $[Ca^{2+}]_i$ was estimated to be 7 μ M (data not shown), which is low compared to other depressing synapses (10–50 μ M) (Schneggenburger and Neher, 2000; Millar et al., 2005). Together with the observation that release is EGTA insensitive, transmitter release from PC terminals is likely regulated by the openings of a low density of tightly coupled Ca^{2+} channels.

We further attempted to validate our estimates of large RRP size and low Pr at PC terminals by using an imaging technique, which had the advantage of being less invasive compared with patch-clamp recordings. For this end, synaptopHluorin (Sankaranarayanan and Ryan, 2001; Fernández-Alfonso and Ryan, 2004) was expressed in a PC, which allowed us to monitor the increase in fluorescence upon vesicle release that results from pHluorin being exposed to the neutral pH of the extracellular space relative to the acidic vesicle lumen. As shown in Figure 3G, 20- or 100-Hz AP trains elicited by somatic depolarization increased the fluorescence in axonal varicosities. Consistent with the frequency-dependent depression of IPSCs, the increase in synaptopHluorin-based fluorescence following 400 APs at 20 Hz was approximately three times larger than that at 100 Hz (Figure 3H, $p < 0.005$). Thus, high-frequency stimulation resulted in depressed synaptic vesicle release, but the availability of vesicles does not seem to be the key determining factor. When acidification of the vesicle lumen following endocytosis was inhibited by bafilomycin, a specific inhibitor of vesicular ATPase (Sankaranarayanan and Ryan, 2001; Fernández-Alfonso and Ryan, 2004), the increase in fluorescence following 400 APs at 20 Hz was augmented by 60%, suggesting that about 40% of released vesicles are endocytosed and re-acidified during the 20 s stimulation period (Figure 3I). In addition, we observed that though vesicle re-cycling was blocked by bafilomycin, the number of remaining vesicles available for release still exceeded the number of vesicles released during the 1st round of 400 APs at both 20 Hz (see Figure 3I) and 100 Hz (not shown), suggesting the number of vesicles is not a key constraint. Taken together, our data suggest that cultured PC terminals have a large releasable synaptic vesicle pool, which is not readily depleted by repetitive AP arrival, and thus is unlikely to limit synaptic transmission.

AP Attenuation around Axon Terminals Weakens Synaptic Transmission

The large RRP and low Pr characteristic of PC axon terminals suggest that the frequency-dependent depression of PC outputs to the target neuron is not mediated by RRP depletion but by some activity-dependent mechanism that limits vesicle release. One obvious candidate is the attenuation of the AP and/or its failure in conduction along the axon or at axon terminals. To test this possibility, we recorded simultaneously from both the axon and its terminal separated by at least 300 μ m (Figures 4A and S3A). APs were evoked at 20, 50, or 100 Hz by either a 2 ms depolarizing pulse (to 0 mV) or a 1 to 2 ms current injection of 200–700 pA (Figure S3C). Supporting our hypothesis, the propagation of APs to the terminal showed either conduction failure (a representative single sweep shown as example 1) or attenuation in the peak amplitude (example 2) in a frequency-dependent manner (20 Hz, $97\% \pm 2\%$ at 20th AP relative to the 1st; 50 Hz, $86\% \pm 7\%$; 100 Hz, $61\% \pm 9\%$, $n = 14$ cells) (Figures 4B and 4C; also see Figure S3D). In contrast, dual recordings of APs from two distinct sites along a single axon (separated by ~ 300 μ m and several branching points, Figure S3B) showed reliable AP propagation (20 Hz, $103\% \pm 2\%$ at 20th AP, $p = 0.1$ by Mann-Whitney U test compared with terminal; 50 Hz, $103\% \pm 3\%$, $p = 0.013$; 100 Hz, $95\% \pm 4\%$, $p = 0.008$, $n = 6$ cells) (Figures 4D–4F). This result is consistent with previous studies of faithful AP

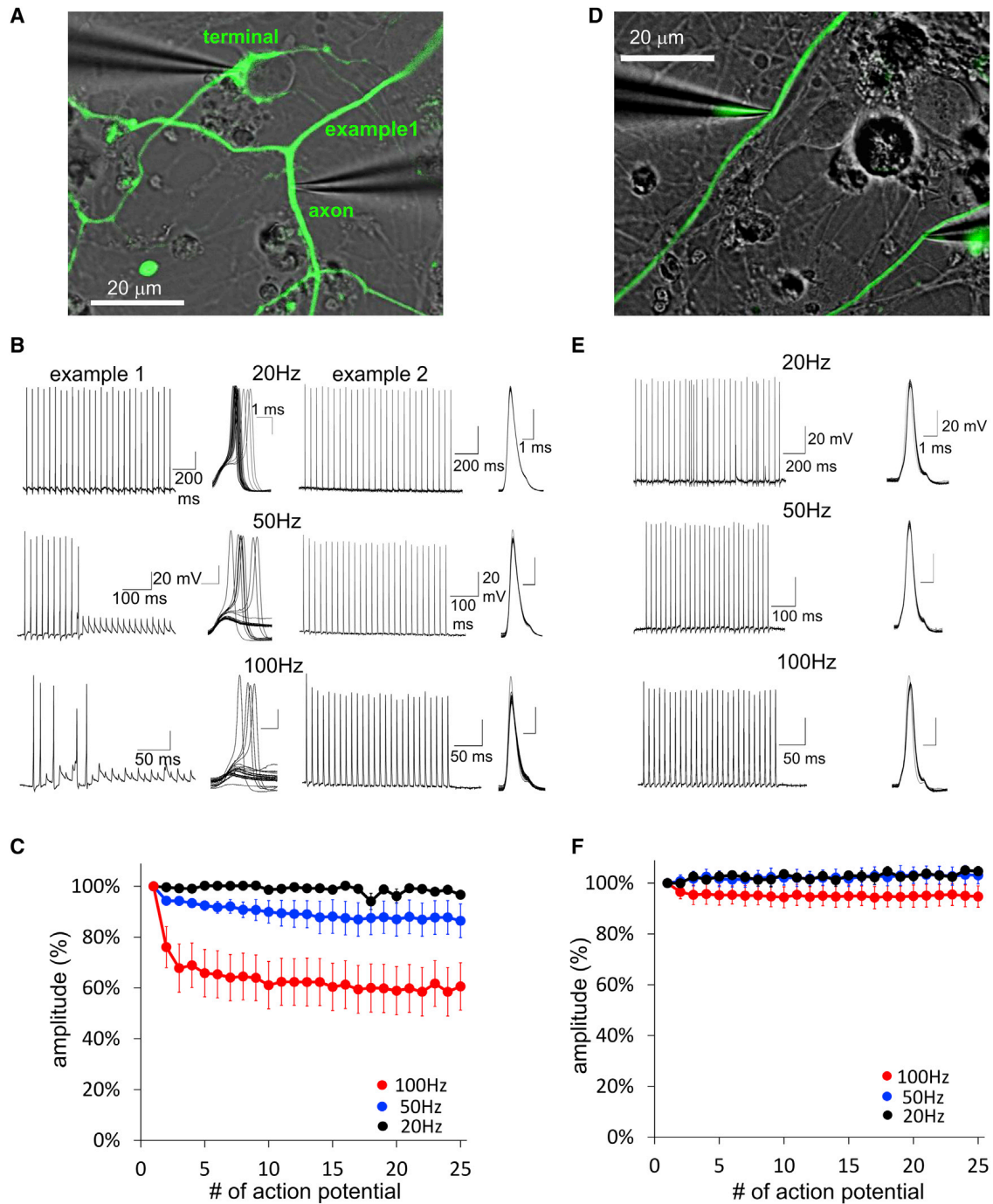


Figure 4. Attenuation of APs at Axon Terminals

(A) An image of a paired recording from an axon and its terminal.

(B) Representative traces of AP trains conducted from the axon to the terminal in two example cells. The recording shown in example 1 corresponds to the image shown in (A). APs were triggered from the patch-clamped axon at frequencies of 20, 50, or 100 Hz.

(C) Peak amplitudes of APs were normalized by that of the first AP (mean \pm SEM); $n = 14$ cells.

(D) An image of paired recordings from two different sites along a single axon.

(E) Representative traces showing AP conduction when evoked by trains of up to 100 Hz at axonal sites.

(F) Plot of AP amplitude normalized to the first; $n = 6$ cells. See also [Figure S3](#).

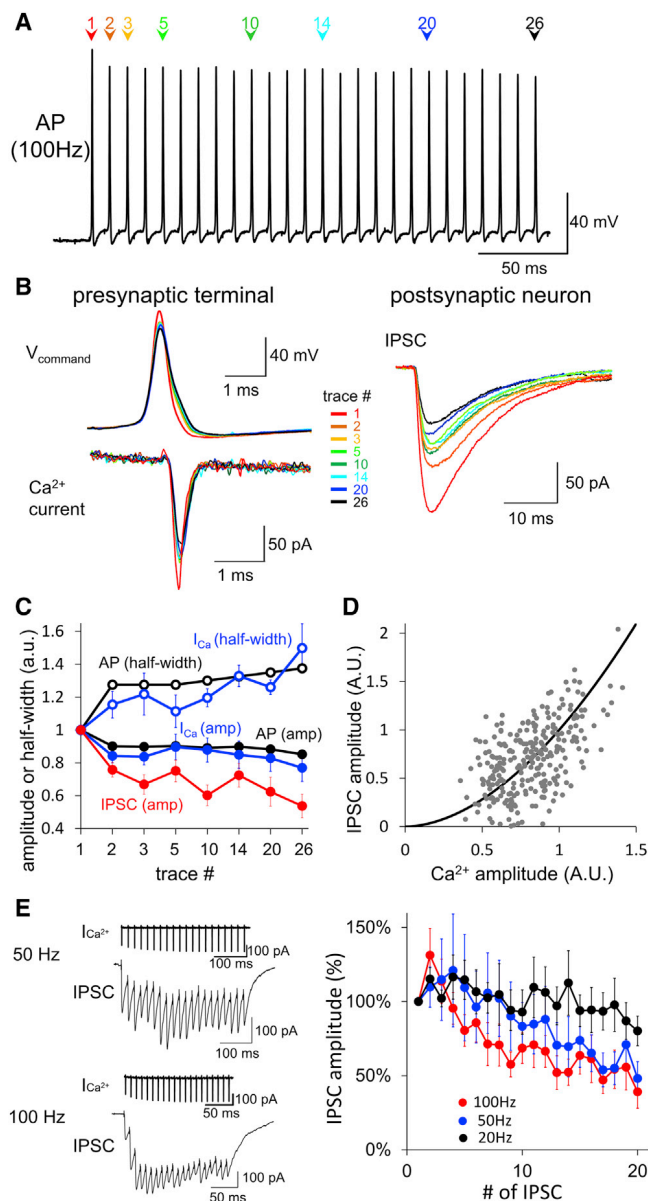


Figure 5. Impact of AP Attenuation on Synaptic Transmission

(A) AP trains recorded from a terminal stimulated at a distant axonal site at 100 Hz. From the AP trains, eight different AP waveforms with different amplitudes (indicated by colored arrowheads) were selected for voltage commands used in (B).

(B) Representative presynaptic Ca^{2+} currents and IPSCs in response to the eight different AP-like voltage commands.

(C) Average plot of AP amplitude, AP half-height width, presynaptic Ca^{2+} current amplitude, presynaptic Ca^{2+} current half-width, and IPSC amplitude in response to the eight different AP-like voltage commands; $n = 6$ cells.

(D) Relationship between IPSC amplitude and Ca^{2+} current. Each gray dot represents individual presynaptic Ca^{2+} current and the resultant IPSC. A black curve represents the relationship between Ca^{2+} and IPSC amplitudes, characterized by a 1.8 power dependency. Peak Ca^{2+} current and IPSC amplitude in each cell were normalized to the average elicited by AP waveform #1.

(E) Left: Representative traces of presynaptic Ca^{2+} currents and IPSC trains elicited by 20 AP-like voltage commands with an identical waveform. Right: IPSC amplitude resulting from trains of identical AP waveforms evoked at 20, 50, or 100 Hz. Data are presented as mean \pm SEM.

conduction along PC axons when recorded extracellularly (Khalil and Raman, 2005; Monsivais et al., 2005). Similarly, when we performed extracellular axonal stimulation and recorded from the terminal, we also observed a frequency-dependent attenuation and/or conduction failure of action sodium currents (Figures S3E–S3G). These results indicate that APs safely propagate along PC axons over many branches but are attenuated around the terminals.

We next examined how the observed AP attenuation affected both the Ca^{2+} influx into the presynaptic terminal and the resulting synaptic transmission (Figure 5). AP waveforms were recorded from PC terminals in response to 100 Hz axonal stimulation (Figure 5A). In this particular case, AP attenuation was modest ($\sim 10\%$). Eight AP waveforms (1st, 2nd, 3rd, 5th, 10th, 14th, 20th, and 26th) are superimposed in Figure 5B (shown as V_{command}). Compared with the first AP, the following APs showed smaller peak amplitudes and greater half-width. We then applied these AP waveforms as voltage commands (stimulated sequentially at 0.5 Hz) to the voltage-clamped presynaptic terminal and observed the subsequent Ca^{2+} currents (Figure 5B). As the amplitude of evoked AP waveform became smaller, so did the Ca^{2+} current amplitude, in a linear fashion (Figures 5B and 5C). In addition, the half-width of Ca^{2+} currents became wider as the AP waveform became wider (Figures 5B and 5C). As was expected, a reduction in the peak Ca^{2+} current was associated with a reduction in the amplitude of evoked IPSCs (Figure 5C). This is consistent with previous studies showing that the Ca^{2+} current amplitude more strongly affects the amount of transmitter release compared to its half-width (Bollmann and Sakmann, 2005). Within the range we examined, transmission at six synapses showed, on average, a $\sim 1.8^{\text{th}}$ power dependency on the Ca^{2+} current amplitude (Figure 5D), similar to previous estimates at other inhibitory presynaptic terminals (Kraushaar and Jonas, 2000; Bucurenciu et al., 2008). To further assess the role of AP attenuation, a train of identical AP waveform commands was applied to the terminal, and the resulting IPSCs were recorded from the postsynaptic neuron. As shown in Figure 5E, direct stimulation of a terminal with such AP trains weakened the depression of IPSCs (20 Hz, $91\% \pm 13\%$, average of 16th–20th IPSCs, $p > 0.6$ compared with control, 50 Hz, $59\% \pm 12\%$, $p > 0.6$, 100 Hz, $52\% \pm 12\%$, $p < 0.05$, $n = 5$ cells) (please compare with Figure 1C). Presynaptic Ca^{2+} currents showed slight facilitation during the train (Figure 5E). On the other hand, when the peak amplitude of AP trains gradually reduced to 60% (similarly to that shown in Figure 4C), the Ca^{2+} current amplitude was reduced to $30\% \pm 11\%$ ($n = 3$) of its initial value (data not shown). Collectively, attenuation of APs during high-frequency stimulation reduces Ca^{2+} influx to the presynaptic terminal, resulting in the depression of IPSCs.

Low Excitability of PC Axon Terminals

Why do APs attenuate in close proximity to the terminals in spite of their successful conduction along the axon across many branch points? To address this question, we compared membrane excitability of an axon and a terminal by direct whole-cell recording of voltage-gated currents (see Supplemental Experimental Procedures for the issue of space-clamp). In response to depolarizing pulses, an axon showed large transient

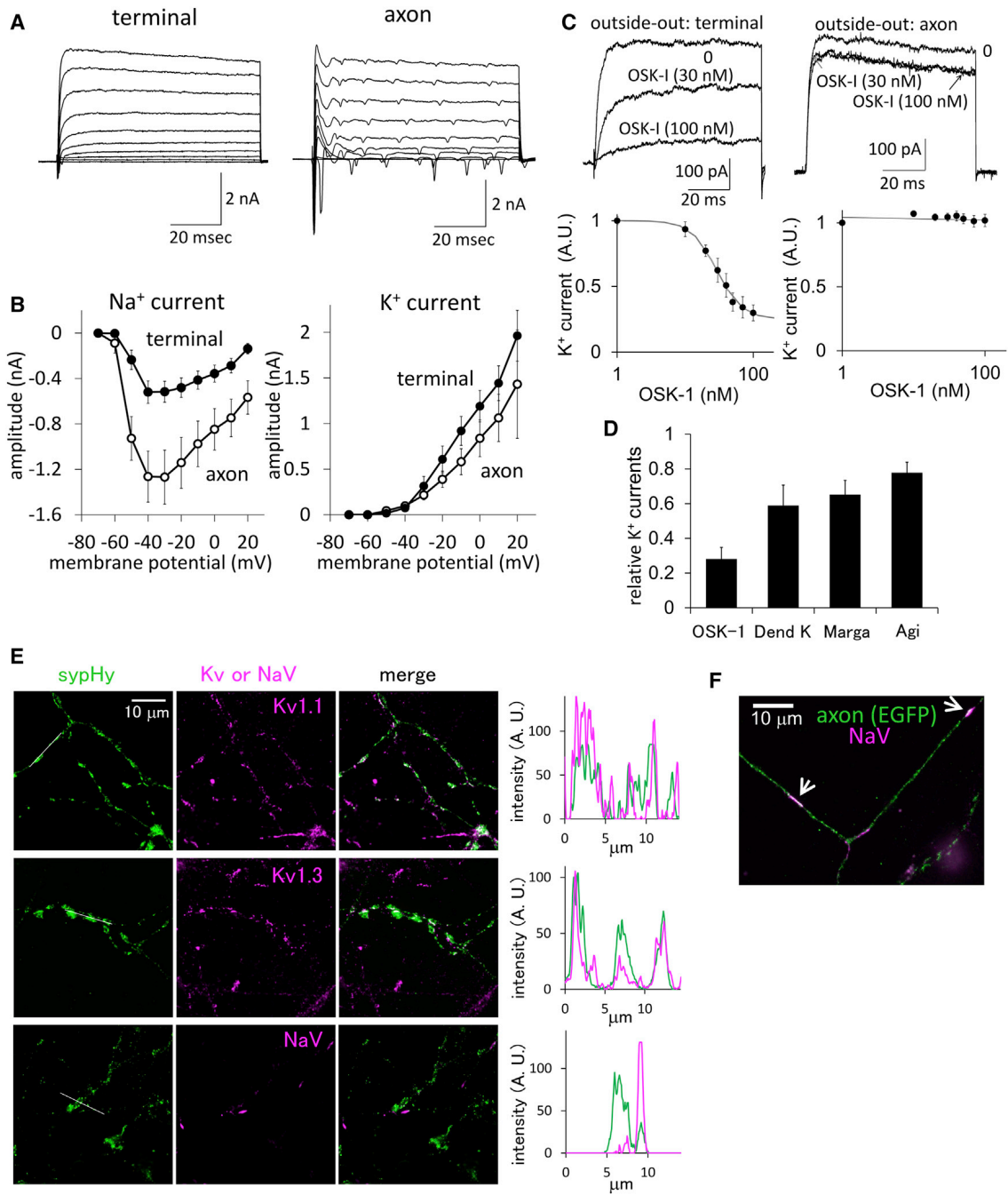


Figure 6. Low Excitability of Presynaptic Terminal Membrane Relative to an Axon

(A) Representative voltage-gated currents recorded from an axon (right) and a presynaptic varicosity (left). Membrane potentials were depolarized with a 10 mV step from -70 mV to $+20$ mV for 80 ms.

(B) Current-voltage relations for voltage-gated Na⁺ (left) and K⁺ currents (right) recorded from an axon (open circles) and a terminal (filled circles); Data are presented as mean \pm SEM. $n = 30$ for terminals and 12 for axons.

(C) Representative traces of voltage-gated K⁺ currents recorded by outside-out membrane patches excised from a terminal (left) and an axon (right) with (30 or 100 nM) or without OSK-1, a peptide inhibitor of Kv-1 family K⁺ channels. Dose-response curves for inhibitory effects of OSK-1 on K⁺ currents are shown at bottom; $n = 3$ for terminal and 4 for axon.

(D) Inhibition of K⁺ currents recorded from excised terminal membrane patches by OSK-1 (100 nM, $n = 3$), Dendrotoxin K (50 nM, $n = 5$), Margatoxin (500 nM, $n = 4$), or Agitoxin (750 nM, $n = 4$).

(E) Immunofluorescent images of synaptophysin-pHluorin (sypHy, green) expressed in PCs and either Kv1.1, Kv1.3, or Na_v (magenta). Line plots of signal intensities along white lines indicated in sypHy images are also shown. To estimate co-localization of each channel with synaptophysin signal, the similarity of signal

(legend continued on next page)

inward currents mediated by voltage-gated Na⁺ channels (1.3 ± 0.2 nA at -40 mV), followed by sustained outward currents through voltage-gated K⁺ channels (1.1 ± 0.3 nA at 10 mV) (Figures 6A and 6B). On the other hand, Na⁺ currents recorded at PC presynaptic varicosities were relatively small (0.5 ± 0.1 nA at -40 mV, $p = 0.008$, Student's *t* test), whereas K⁺ currents tended to be large (1.4 ± 0.2 nA at 10 mV) (Figures 6A and 6B). It should be noted that the Na⁺ current amplitude might be slightly underestimated at positive membrane potentials due to the large K⁺ conductance (see Figure S4A). Thus, the terminal appears able to conduct little Na⁺ current relative to its large K⁺ permeability. Given that the Na⁺/K⁺ conductance ratio determines the membrane excitability, we predict the terminal to be relatively less excitable. In accordance with the data, immunocytochemistry demonstrated that Na⁺ channels were accumulated at specific parts of the axon, which were likely the nodes of Ranvier (Figure 6F), but exhibited sparse labeling at the terminals (Figure 6E). Consistently, compared with axons, axon terminals did not exhibit AP firing in response to current injection (18 out of 30 cells), presumably because of their weak Na⁺ conductance relative to the large shunting effect by K⁺ channels (Figure S4B). Direct recording from a PC axon terminal in slice showed similar results and is consistent with low excitability of the terminal (see Figure 8 and S6). To summarize, axon terminals are less excitable than the axon, which leads to the attenuation of APs.

Low Terminal Excitability Responsible for Frequency-Dependent Synaptic Depression

To test whether the low excitability of an axon terminal underlies the depressive property of PC terminal synapses, we searched for a pharmacological agent to increase the excitability of the terminal but not the axon. For this, we performed outside-out recordings of voltage-gated currents from membrane patches excised from either the terminal or axon. As shown in Figure 6C, the voltage-gated K⁺ current recorded from a terminal patch was attenuated by application of OSK-1, an inhibitor of the Kv1 family (Kv1.1, Kv1.2, and Kv1.3) of voltage-gated K⁺ channels ($29\% \pm 6\%$ of basal at 100 nM). In contrast, OSK-1 did not affect the K⁺ current recorded from the axonal membrane ($100\% \pm 18\%$ of basal, $p = 0.027$, Student's *t* test compared with terminal) (Figure 6C). Thus, the composition of voltage-gated K⁺ channels differs between the axon and the terminal. In addition, the voltage-gated K⁺ current recorded from the terminal was inhibited by 50 nM of the Kv1.1 and 1.2 blocker Dendrotoxin K, ($59\% \pm 12\%$, $n = 5$), 500 nM of the Kv1.3 blocker Margatoxin ($65\% \pm 8\%$, $n = 4$), and 750 nM of the Kv1.3 blocker Agitoxin ($78\% \pm 6\%$, $n = 4$) (Figure 6D). Because the K⁺ conductance in the terminal was highly sensitive to 2 mM TEA (not shown), Kv1.2 seemed not to be involved. Taken these results together, Kv1.1 and Kv1.3 are likely to be the predominant subtypes that mediate the voltage-gated K⁺ current at PC terminals. Accordingly, immunocytochemistry showed localization of both Kv1.1 and Kv1.3 at PC axonal varicosities (visualized by sypHy, synap-

tophysin tagged with a GFP variant pHluorin), but not at axonal locations (Figure 6E). The area positive for sypHy was also positive for VGAT (not shown). Intensity profiles in the line scan showed colocalization of sypHy with Kv, but not Nav_v (Figure 6E). Rather, Nav_v was mainly localized in the axon (Figure 6F).

In the following sets of experiments, we confirmed that OSK-1 suppresses AP attenuation by selectively altering membrane excitability. First, recordings from the terminal showed that OSK-1 weakened the extent of frequency-dependent AP attenuation ($n = 4$, data not shown) without affecting the resting membrane potential of the terminal (before, -69 ± 2 mV; after OSK-1 application, -68 ± 2 mV, $p = 0.82$, $n = 4$). Second, Ca²⁺ imaging using Oregon green BAPTA-1 (500 μ M applied to a PC soma through a patch pipette) demonstrated that the Ca²⁺ increase around the terminals following 100 APs at 100 Hz was augmented by OSK-1 application (Figure S5). Importantly, the augmenting effect of OSK-1 became evident not at the beginning of the AP train, but at later points during the stimulation. Thus, the Ca²⁺ imaging data further suggests that OSK-1 weakened the high-frequency-dependent negative regulation of AP and the resulting reduction in presynaptic Ca²⁺ influx.

We next examined how the increase in presynaptic excitability by 20 nM OSK-1 affected the frequency-dependent depression of synaptic transmission at PC synapses. As shown in Figures 7A and 7B, depression of synaptic transmission upon 50 Hz stimulation of the PC soma was almost abolished by OSK-1 treatment ($84\% \pm 6\%$, average of 16^{th} – 20^{th} IPSCs, $p = 0.007$, Student's *t* test compared with control). Similarly, in response to 100 Hz trains, the synaptic depression was also markedly reduced by OSK-1 ($54\% \pm 8\%$, $p = 0.0003$). Thus, increased membrane excitability by inhibition of K⁺ channels in the presynaptic terminal weakened frequency-dependent depression of IPSCs. These results were in accord with the idea that the AP attenuation around the presynaptic terminals contributed to depression of synaptic transmission. Temperatures may affect electrical and synaptic properties (Kushmerick et al., 2006; Fernández-Alfonso and Ryan, 2004), but the frequency-dependent depression of IPSC was also evident at physiological temperature (32°C – 34°C) (20 Hz, $87\% \pm 3\%$, average of 16^{th} – 20^{th} IPSCs; 50 Hz, $81\% \pm 5\%$; 100 Hz, $30\% \pm 7\%$; 200 Hz, $11\% \pm 3\%$) and was suppressed by inhibition of Kv1 channels with OSK-1 (20 Hz, $87\% \pm 7\%$; 50 Hz, $71\% \pm 5\%$; 100 Hz, $59\% \pm 5\%$, $p < 0.001$ compared with control; 200 Hz, $30\% \pm 6\%$, $p < 0.05$) (Figure 7C). Under physiological temperature, we also found attenuation of APs at the presynaptic terminal when an axon was stimulated at 100 Hz ($n = 3$).

Low Presynaptic Excitability Determines Synaptic Depression in Acute Slices at Multiple Types of Synapse

We next attempted to confirm our results at PC-DCN synapses in acute slices prepared from postnatal day 9–16 rats. To examine the excitability of the terminal, we fluorescently labeled PC axons in the DCN with DiO (0.5% in external solution) applied locally to

distribution pattern was assessed by calculating the Pearson product-moment correlation coefficient, which ranges between -1 and 1 (higher value represents higher co-localization; Kv1.1, 0.55 ± 0.15 ; Kv1.3, 0.64 ± 0.09 ; Nav_v, 0.23 ± 0.11 ; $p < 0.05$).

(F) Immunocytochemistry for Nav_v (magenta) and EGFP (green, a PC axon). High signals for Nav are observed in an axon as white or magenta signals (highlighted by white arrows). See also Figure S4.

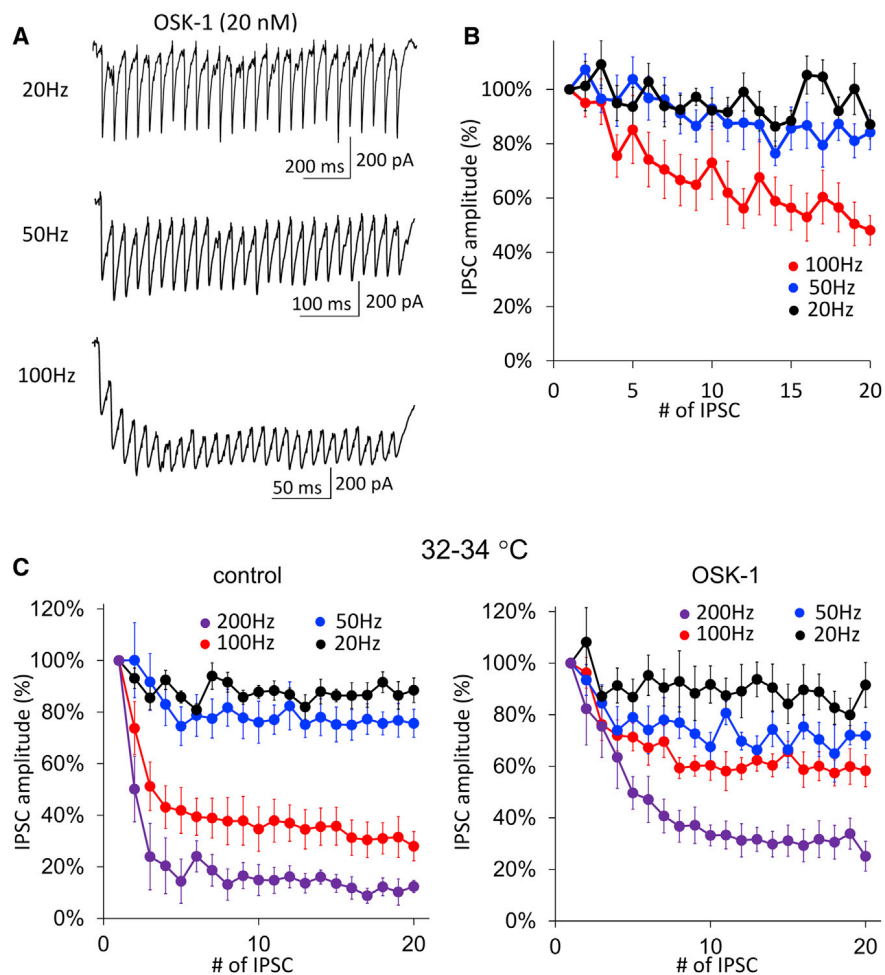


Figure 7. Frequency-Dependent Depression of IPSCs Was Attenuated by Blocking Terminal-Specific Voltage-Gated K⁺ Channels

(A) Representative traces of IPSC trains (averaged from 20 traces) stimulated at 20, 50, or 100 Hz in the presence of 20 nM OSK-1. IPSCs were triggered from PC soma in the whole-cell configuration.

(B) IPSC amplitudes were normalized to that of the first; $n = 8$. The effect of OSK-1 can be assessed by comparing the data to that performed in the absence of OSK-1 (shown in Figure 1C).

(C) Plot of average IPSC amplitudes evoked by train stimulation at 20, 50, 100, and 200 Hz with (right) or without (left) 20 nM OSK-1 at 32°C–34°C; $n = 8$ in control conditions, except for 200 Hz ($n = 5$); $n = 5$ for OSK-1-treated recordings. Data are presented as mean \pm SEM. See also Figure S5.

the white matter of sagittal cerebellar slices through a glass pipette (for 30 min). Once the PC axons could be visualized, we performed direct patch-clamp recordings from the terminals (Figure 8A). It was likely that we recorded from presynaptic terminals, because Cm jumps were observed in response to depolarizing pulses though, notably, the peak Cm was smaller than in the culture preparation (Figure S6A). APs were elicited at a frequency of 100 Hz by extracellular electrical stimulation (100 μ sec) through a glass electrode placed in the white matter. Although APs were reliably recorded at the beginning of trains, they tended to fail over the course of stimulation, in line with our observations in culture. On average ($n = 5$), the success probability of presynaptic spikes dropped by 40%–50% during 100 Hz train stimulation (Figure 8B).

Next, we examined whether weak excitability of PC axon terminals mediated frequency-dependent depression of synaptic transmission in situ. Whole-cell recordings were made from a neuron with a large cell body (>15 μ m diameter), and evoked IPSCs were recorded following electrical stimulation in the white matter. Consistent with previous studies, IPSCs from PC axon terminals were identified by their characteristic all-or-none response to increasing stimulation intensity and their relatively large amplitude (Telgkamp and Raman, 2002; Pedroarena and

Schwarz, 2003). IPSC amplitudes were somewhat larger in slice recordings, which may be due to multiple varicosities along an axon innervating a single post-synaptic neuron. However, we do not exclude the possibility that Pr was somewhat higher in slices. Because cultured PC axon terminals fired at \sim 5 Hz at rest (see Figure S6), test stimulations of 20, 50, or 100 Hz were applied to the white matter following 10 pre-stimulations at 5 Hz. In accordance with previous studies (Telgkamp and Raman, 2002; Pedroarena and Schwarz, 2003), recordings of IPSCs at PC-DCN synapses in acute slices exhibited similar frequency-dependent depression to that observed at cultured PC outputs (20 Hz, 66% \pm 11%, average of 16th–20th IPSCs; 50 Hz, 28% \pm 11%; 100 Hz, 16% \pm 5%) (Figure 8). After application of 50 nM OSK-1, IPSC amplitude was increased by 1.72 \pm 0.31 fold, and the subsequent IPSCs were all larger than the original level. If depletion of the RRP was responsible for the extent of synaptic depression, the increase in the 1st IPSC amplitude would lead to decrease of the amplitude of subsequent IPSCs, and hence enhance the short-term depression. In contrast, we observed that the synaptic depression induced by repetitive stimulation was weakened by treatment of OSK-1 (20 Hz, 77% \pm 6% at 20th IPSC, $p = 0.11$ by paired t test compared with basal; 50 Hz, 47% \pm 15%, $p = 0.012$; 100 Hz, 27% \pm 9%, $p = 0.019$) (Figure 8). Such data support the idea that low membrane excitability of PC axon terminals contributed to frequency-dependent depression. Without pre-stimulation, the depression of IPSC trains relative to the first IPSC was stronger (10 Hz, 40% \pm 4%, average of 16th–20th IPSCs; 20 Hz, 30% \pm 2%; 50 Hz, 17% \pm 2%; 100 Hz, 11% \pm 1%, Figure S6), in accordance with previous studies (Telgkamp et al., 2004). In this condition, 50 nM OSK-1 weakened IPSC depression when the stimulation frequency was set to either 10 Hz (55% \pm 5%, $p = 0.004$ by paired t test), 20 Hz

(42% ± 4%, $p = 0.004$), or 50 Hz (22% ± 2%, $p = 0.038$), but not during 100 Hz stimulation (11% ± 1%, $p = 0.5$, Figure S6). The absence of OSK-1-mediated effect at 100 Hz might be possibly due to a K^+ -channel-independent mechanism that favorably operates even at relatively low stimulation frequencies.

It is possible that K^+ channel blockade increased Ca^{2+} influx, thereby augmenting Ca^{2+} -dependent synaptic vesicle replenishment (Dittman and Regehr, 1998; Stevens and Wesseling, 1998). However, while increasing external Ca^{2+} concentration from 2 to 4 mM increased the IPSC amplitude (1.99 ± 0.19 times), similar to OSK-1, the depression of IPSC amplitude during train stimulation did not markedly change (Figure S6H). To summarize, low excitability of PC axon terminals enriched with OSK-1-sensitive Kv1.1 and Kv1.3 channels underlies the depression of PC outputs. In contrast, depletion of the RRP appears to play no major role at this synapse.

Finally, we tested whether weak membrane excitability also causes synaptic depression at other inhibitory synapses. We performed paired recordings from cerebellar fast-spiking BCs and PCs at physiological temperature. A 100 Hz train of presynaptic stimulation (0 mV for 2 ms) caused synaptic depression at this inhibitory connection (Vincent and Marty, 1996; Sakaba, 2008). Application of TEA (10 mM), a K^+ channel blocker, augmented the first IPSC amplitudes to 234% ± 57% ($n = 6$) and, importantly, converted synaptic depression into facilitation (Figure 8F, $p < 0.01$). If RRP depletion primarily mediates the depression, an increase in the Pr should have augmented the depression. The results are similar to the PC-DCN synapse and consistent with the idea that excitability controls synaptic depression. Accordingly, extracellular recordings of AP trains at 50 and 100 Hz showed that the AP amplitude tended to be attenuated (Figure S6I). AP propagation along the axon is reported to be reliable in fast-spiking neurons (Hu and Jonas, 2014), and hence, AP attenuation is likely to occur around the terminals.

We also recorded IPSCs from cultured hippocampal neurons where release-independent depression has been previously suggested (Kraushaar and Jonas, 2000). As shown in Figure 8G, IPSCs were strongly depressed upon repetitive stimulation. Interestingly, inhibition of K^+ channels by 10 mM TEA weakened the high-frequency-dependent depression (20, 50, and 100 Hz, $p < 0.05$) but did not affect synaptic depression when stimulation frequency was lowered to 10 Hz (data not shown). It should be noted that unlike PC output synapses, the normalized IPSC amplitudes after the 8th stimulation became similar to those without TEA treatment, suggesting that the RRP would be depleted after high-frequency stimulation.

Taken these results together, low presynaptic membrane excitability contributes to depression of inhibitory synaptic transmission not only in cerebellar PCs but also in cerebellar BCs and hippocampal neurons.

DISCUSSION

By developing a technique to directly record from inhibitory presynaptic terminals of cultured cerebellar PCs, we have demonstrated an information processing mechanism that occurs in close proximity to axon terminals. By taking advantage of a cere-

bellar culture preparation and aided by visualization of axons and small terminals expressing EGFP, we succeeded in overcoming the difficult task of direct recordings from axons and small varicosities (1–3 μm) (but see Novak et al., 2013). This technique allowed us to reveal a series of findings. (1) We demonstrated the basic mechanism of transmitter release at an inhibitory terminal. Measurement of presynaptic Cm, deconvolution of evoked IPSCs, and Ca^{2+} uncaging revealed the presence of a large pool of releasable vesicles, of which <1% were exocytosed upon a single AP. (2) We identified low membrane excitability to be a key determinant of short-term depression. Paired patch-clamp recordings from an axon and a terminal demonstrated that APs were conducted reliably along the axon and over bifurcations, but tended to be attenuated around terminals. This resulted in a reduction of Ca^{2+} influx within the terminal, thus causing weaker synaptic transmission. Our data further suggest that the low membrane excitability of axon terminals resulted from sparse expression of Na^+ channels relative to the abundant localization of the Kv1-family of voltage-gated K^+ channels. Inhibition of terminal K^+ channels suppressed the frequency-dependent depression of PC outputs in both culture and slice. Moreover, overall results were confirmed by a less invasive, imaging approach. Thus, our data show that information conducted along an axon is subject to frequency-dependent modulation at sites close to terminals and is then transmitted to postsynaptic neurons with altered strength.

The RRP at PC Terminals

The RRP of synaptic vesicles and the kinetics of transmitter release have been measured at excitatory synapses where Cm measurements and simultaneous recordings from presynaptic and postsynaptic compartments are possible (von Gersdorff and Matthews, 1994; Sun and Wu, 2001; Hallermann et al., 2003). In spite of the important roles of inhibitory synapses in information processing in the circuit (Lawrence and McBain, 2003; Jonas et al., 2004), a study of inhibitory terminals has been lacking. Here we have simultaneously measured the presynaptic Cm and IPSCs from PC output synapses that exhibit frequency-dependent depression. Postsynaptic GABA receptors tend to be saturated or desensitized at inhibitory synapses (Pugh and Raman, 2005); therefore, we used presynaptic Cm measurements that reflect exocytosis of synaptic vesicles more reliably. Surprisingly, we observed a very large RRP (>1,000 vesicles) with an extremely low Pr (~0.005). At most excitatory and inhibitory synapses that undergo depression, Pr has been considered to be relatively high (>0.1) (Kraushaar and Jonas, 2000), and depletion of the RRP considered to determine the time course of synaptic depression during a train of APs (Saviane and Silver, 2006). In contrast, the RRP size is large and Pr low at facilitating synapses (Millar et al., 2005; Hallermann et al., 2003). The PC synapse is surprising in this respect, because this depressing synapse has a low Pr and a large RRP, typical features of facilitating synapses. Nevertheless, the observation is consistent with morphological data at the PC output synapse and other inhibitory synapses, where the release sites are less well defined but accumulation of synaptic vesicles are observed (Telgkamp et al., 2004; Palay and Chan-Palay, 1974).

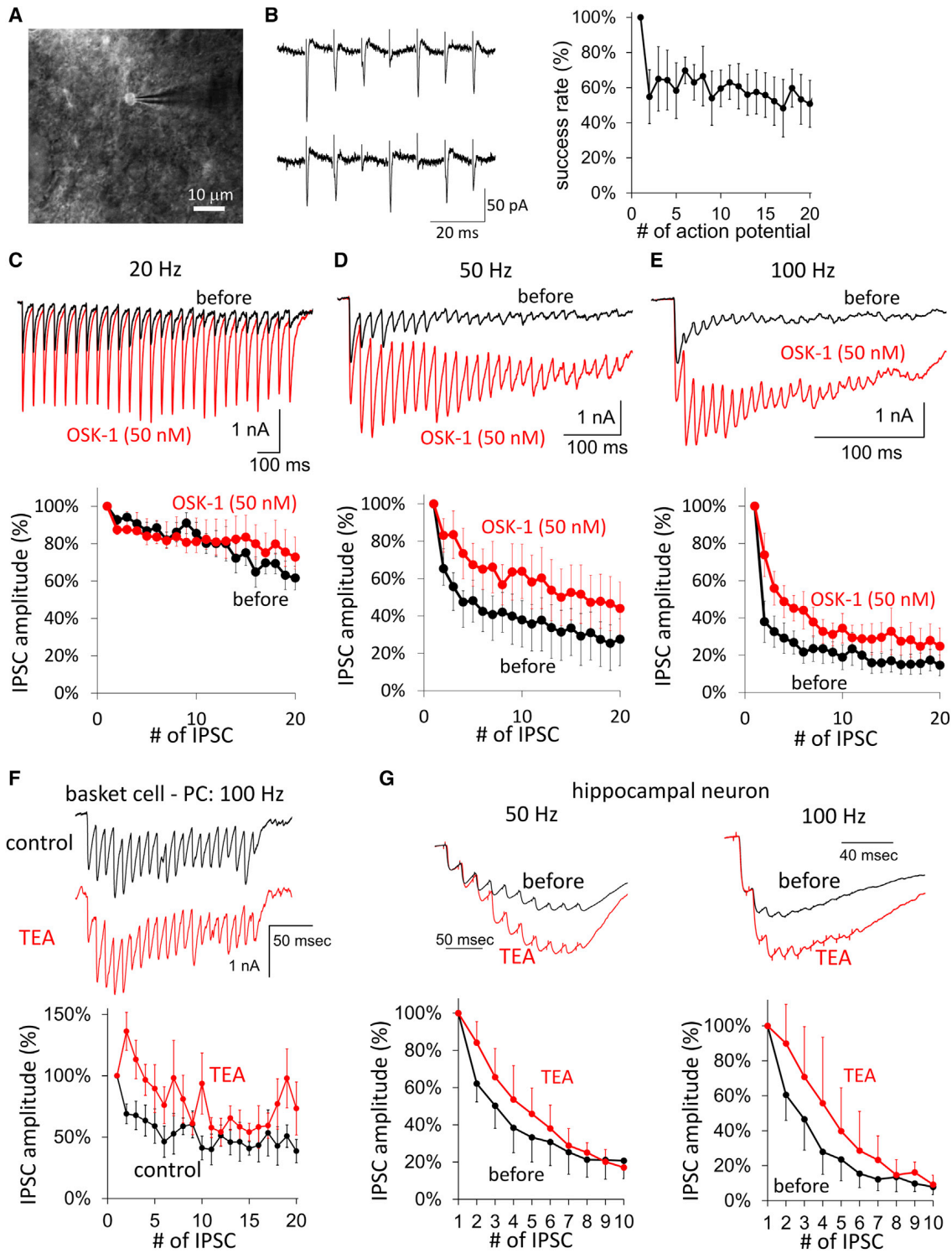


Figure 8. IPSC Depression at PC-DCN Synapses in Cerebellar Slices Was Suppressed by K^+ Channel Blockade

(A) An image of a patch-clamped PC varicosity visualized by DiO applied to the white matter of a cerebellar slice.

(B) Left: Example traces of extracellular spike recordings from a PC terminal upon the white matter stimulation at 100 Hz. Right: Average success rate of pre-synaptic spikes during a 100 Hz train was plotted against stimulus number.

(C-E) Representative traces (average of 10 traces) and amplitudes of IPSC trains, normalized to the first, stimulated at 20 (C), 50 (D), and 100 Hz (E) before (black) and after (red) OSK-1 (50 nM) application. Prior to train stimulation, PC axons were stimulated ten times at 5 Hz to mimic spontaneous firing in a cultured PC (4–6 Hz); $n = 7$.

(legend continued on next page)

The time constant of the RRP depletion at PC synapses was slower than the 0.5–3 ms previously observed for glutamatergic synapses (Sun and Wu, 2001; Hallermann et al., 2003; Sakaba and Neher, 2001; Mennerick and Matthews, 1996). Slow release from the PC synapse is consistent with a low Pr under basal conditions. Because the Ca^{2+} sensitivity for release is similar to that at excitatory synapses, the low Pr of PC synapses could be explained by a relatively small number of Ca^{2+} channels at release sites during an AP, or by weaker coupling between Ca^{2+} channels and release machinery. The EGTA insensitivity of release suggests that Ca^{2+} channels are coupled tightly to synaptic vesicles, but that the peak $[\text{Ca}^{2+}]_i$ is much lower than that postulated at other inhibitory synapses (Bucurenciu et al., 2008; Sakaba, 2008). While this study shows that release probability per synaptic vesicle is low, it is consistent with the finding that release probability per synapse is high (Telgkamp et al., 2004). The low Pr of a PC terminal contrasts to the relatively high Pr at inhibitory synapses formed by fast-spiking interneurons, as was demonstrated by both statistical analysis of IPSCs (Kraushaar and Jonas, 2000) and analysis using Ca^{2+} uncaging (Sakaba, 2008). However, no direct measurements of exocytosis have been performed at these synapses so far, and thus it remains to be investigated whether the low Pr and large RRP are general features of inhibitory synapses or unique features at PC synapses.

The Mechanisms of Synaptic Depression at the PC Output Synapse

Short-term synaptic depression is seen at many central synapses. At glutamatergic synapses, the RRP depletion is considered to be one of the major mechanisms of depression (Zucker and Regehr, 2002), though other mechanisms such as Ca^{2+} current inactivation and AP conduction failure at axonal branches also contribute (Xu and Wu, 2005; Brody and Yue, 2000; Prakriya and Mennerick, 2000). Characteristics of inhibitory synapses are clearly different from those of excitatory synapses. For example, depression time course is relatively insensitive to changes in the initial Pr, which can be caused by alterations in the external $[\text{Ca}^{2+}]$ (Kraushaar and Jonas, 2000). In contrast, glutamatergic synapses show deeper depression at higher Pr (Dittman and Regehr, 1998). Thus, it was hypothesized that inhibitory synapses either have a release-independent component of synaptic depression or are engendered with special release mechanisms (Kraushaar and Jonas, 2000; Kirischuk et al., 2002; but see Moulder and Mennerick, 2005). By direct recordings from axons and terminals, we have identified the release-independent mechanism of synaptic depression, that low membrane excitability specifically at the terminal, but not the axon, attenuates the presynaptic AP waveform. Axonal branch failure (Brody and Yue, 2000; Prakriya and Mennerick, 2000) is unlikely to contribute to the depression because of the high reliability of AP conduction in PC axons (Khaliq and Raman, 2005; Monsivais et al., 2005), a finding that we confirmed using dual recordings

from two different sites along the axon. Due to the non-linear dependence of transmitter release on Ca^{2+} , attenuation of APs is a powerful mechanism of synaptic depression, though we emphasize the importance of other depression mechanisms previously identified at this synapse (Telgkamp et al., 2004).

We propose that the low membrane excitability causing the synaptic depression at PC axon terminals was due to a relatively low Na^+ channel number and an abundance of K^+ channels. This contrasts with the view that synaptic depression is generally mediated by vesicle pool depletion, release site inactivation, or Ca^{2+} channel inactivation, which all assume that APs are conducted faithfully to the terminal (Fioravante and Regehr, 2011). Because a release-independent component of synaptic depression is observed in many inhibitory synapses, one may speculate that low excitability may be a general feature of inhibitory terminals. Consistently, we have shown that K^+ channel blockers weakened synaptic depression both at the BC-PC synapses in acute cerebellar slices and at cultured hippocampal inhibitory synapses. We should note that AP attenuation is less drastic at BC terminals compared with PC terminals (Figure S6), and the impact of excitability over other factors might differ between synapse types.

Sparse Na^+ channel clustering in axon terminals has also been reported in other preparations such as the calyx of Held (Leão et al., 2005) and at the neuro-muscular junction (Lindgren and Moore, 1989). The axon heminode near the terminal has abundant Na^+ channels, yet the terminal does not, which might also contribute to low membrane excitability around the terminal. Nevertheless, large Na^+ currents originating from the heminode can be measured at the calyx terminal, thus ensuring reliable AP firing. Absence of Na^+ channels in the terminals seems to limit the duration of APs. Reduction of Na^+ currents by TTX greatly diminishes the EPSCs (Wu et al., 2004), suggesting that the ratio of Na^+ currents over K^+ currents crucially determines the fidelity of AP firing and synaptic transmission at the calyx synapse. K^+ channel expression at the calyx synapse is strong but is considered to shorten the AP waveform rather than causing the AP attenuation. Taken together, large Na^+ and K^+ currents around the calyx of Held terminal contribute to reliable and fast AP firing up to kHz frequencies (Taschenberger and von Gersdorff, 2000). En-passant-type mossy fiber terminals in hippocampus, another model system of glutamatergic terminals, express abundant Na^+ and K^+ channels (Engel and Jonas, 2005; Geiger and Jonas, 2000), which amplify the presynaptic AP amplitude and limit the AP duration. Cerebellar mossy fiber terminals also have abundant Na^+ and K^+ channels and follow APs up to hundreds of Hz (Rancz et al., 2007). Therefore, the localization pattern of Na^+ and K^+ channels around terminals impacts the reliability of presynaptic AP firing and synaptic transmission.

Physiological Implications

PCs provide the sole output from the cerebellar cortex and are considered to form strong inhibitory synapses onto DCN

(F and G) Top panels show representative traces of IPSCs at BC-PC synapses (F) and at cultured hippocampal inhibitory synapses (G) (average of 10–30 traces) with (red) and without (black) 10 mM TEA. The presynaptic neuron was stimulated at 50 or 100 Hz by depolarizing the soma to 0 mV for 2 ms. Bottom panels show the amplitude of IPSC trains (normalized to the 1st amplitude), with (red) and without (black) TEA. Differences between the two plots were statistically significant ($p < 0.01$ in [F] and $p < 0.05$ in [G]). To isolate the high-frequency component of depression in hippocampal neurons, pre-stimulation (five pulses at 10 Hz) was applied before the train stimulation (50 or 100 Hz). Error bars represent SEM. See also Figure S6.

neurons. Axonal AP conduction was shown to be reliable up to hundreds of Hz (Khaliq and Raman, 2005; Monsivais et al., 2005). However, the properties of axon terminals have not been examined in depth. Synaptic strengths under low frequency stimulation seem to be reliable at this synapse. Reliability is aided by multivesicular release, spillover of transmitter, post-synaptic saturation (Telgkamp et al., 2004), as well as a large RRP size (this study). As a consequence of the large RRP size and low Pr, the vesicle pool is kept far from depletion (Kraushaar and Jonas, 2000; Taschenberger and von Gersdorff, 2000). More importantly, synaptic strength becomes very unreliable at high-frequency stimulation, as shown in this study.

What is the advantage of such a synaptic design with low excitability, low Pr, and a large RRP? We consider three possibilities. First, regulation of excitability might be an easy method to establish target-dependent differences in synaptic strengths and plasticity. In addition to the DCN, PC axons make synapses within other regions such as the vestibular nucleus (Shin et al., 2011) as well as other PCs (Orduz and Llano, 2007), where short-term facilitation takes place. Facilitation at such synapses might be due to a greater expression of Na⁺ channels. Inhibition of K⁺ channels by OSK-1 makes the frequency-dependent depression at the PC-DCN synapse somewhat frequency-independent between 20 and 100 Hz (see Figure 7), similar to synapses in the vestibular nucleus where PCs also make an inhibitory contact (Bagnall et al., 2008). As a second possibility, low Pr may support transmission under high rates of spontaneous firing. Low Pr and large RRP may limit the extent of synaptic vesicle depletion and support transmission during long-lasting stimulation (Kraushaar and Jonas, 2000; Taschenberger and von Gersdorff, 2000). Because basal firing frequency is high in vivo and dynamically changes during motor control (Loewenstein et al., 2005), the filtering characteristics are functionally important. The frequency-dependent depression due to the low excitability of pre-synaptic boutons might function to fine-tune the working range of postsynaptic neuronal activity, without depleting the presynaptic RRP. As a third possibility, a large RRP may allow room for short- and long-term synaptic plasticity, and vesicle pool depletion may become rate limiting only after induction of plasticity.

Potent inhibition of the postsynaptic DCN neurons caused by burst firing of PCs is followed by a rebound depolarization, accompanied by an increase in [Ca²⁺]_i. This inhibition-triggered rebound depolarization leads both to synaptic plasticity at the homosynaptic PC synapses (Aizenman et al., 1998) and modulation of plasticity at excitatory mossy fiber synapses (Pugh and Raman, 2006). Thus, frequency-dependent signal modulation around axon terminals might play a role in adaptive changes of neuronal processing in the DCN. It remains to be investigated how the characteristic information processing at PC axon terminals affects the overall neuronal computation in the cerebellar networks in vivo.

EXPERIMENTAL PROCEDURES

Animal experiments were performed in accordance with the guidelines regarding care and use of animals for experimental procedures of the NIH (U.S.A.) and Doshisha University and were approved by the local committee for handling experimental animals in Doshisha University.

Culture and Slice Preparation

The method for preparing primary cultures of cerebellar neurons and cerebellar sagittal brain slices were similar to those in previous studies (Kawaguchi and Hirano, 2007; Sakaba, 2008). Hippocampal neurons were cultured in Neurobasal medium (GIBCO) with B27 supplement (GIBCO), and used for experiments 10–16 days after plating.

DNA Construction and Transfection

CAG promoter-based AAV vector (Kaneko et al., 2011) for EGFP transfection was a generous gift from Dr. Kengaku (Kyoto University). cDNAs of sypHy and synaptotagmin were obtained from Addgene (plasmid #24478) and from Dr. T. Hirano (Kyoto University). Transfection was performed by direct micro-injection of cDNA into the nucleus of a PC through a sharp glass pipette or by AAV infection.

Electrophysiology

Electrophysiological experiments were performed similarly to previous studies (Kawaguchi and Hirano, 2007; Sakaba, 2008) at room temperature (20°C–24°C) or at physiological temperature (32°C–36°C). Cm measurements were carried out using sine + DC technique (Neher and Marty, 1982). The deconvolution analysis and Ca²⁺ uncaging were performed as previously described (Sakaba, 2008). For details, see Supplemental Information.

Statistics

Data are presented as mean ± SEM. Statistical significance was assessed by paired t test, unpaired Student's t test, Mann-Whitney U test or ANOVA.

SUPPLEMENTAL INFORMATION

Supplemental Information includes six figures and Supplemental Experimental Procedures and can be found with this article online at <http://dx.doi.org/10.1016/j.neuron.2015.02.013>.

ACKNOWLEDGMENTS

We thank to Dr. T. Takahashi, Y. Goda, M. Rigby, and M. Midorikawa for critical reading of the manuscript and helpful comments. This work was supported by JSPS/MEXT KAKENHI Grant Numbers 24300144, 24650218, and 26110720 to T.S.; 25870895 to S.K.; JSPS Core-to-Core Program A Advanced Research Networks to T.S.; the Toray Science Foundation (T.S.); the Uehara Foundation (T.S.); and the Naito Science Foundation to S.K.

Received: January 27, 2014

Revised: August 6, 2014

Accepted: February 4, 2015

Published: February 26, 2015

REFERENCES

- Abbott, L.F., and Regehr, W.G. (2004). Synaptic computation. *Nature* 431, 796–803.
- Aizenman, C.D., Manis, P.B., and Linden, D.J. (1998). Polarity of long-term synaptic gain change is related to postsynaptic spike firing at a cerebellar inhibitory synapse. *Neuron* 21, 827–835.
- Auger, C., and Marty, A. (2000). Quantal currents at single-site central synapses. *J. Physiol.* 526, 3–11.
- Bagnall, M.W., McElvain, L.E., Faulstich, M., and du Lac, S. (2008). Frequency-independent synaptic transmission supports a linear vestibular behavior. *Neuron* 60, 343–352.
- Bollmann, J.H., and Sakmann, B. (2005). Control of synaptic strength and timing by the release-site Ca²⁺ signal. *Nat. Neurosci.* 8, 426–434.
- Bollmann, J.H., Sakmann, B., and Borst, J.G. (2000). Calcium sensitivity of glutamate release in a calyx-type terminal. *Science* 289, 953–957.

- Borst, J.G., Helmchen, F., and Sakmann, B. (1995). Pre- and postsynaptic whole-cell recordings in the medial nucleus of the trapezoid body of the rat. *J. Physiol.* **489**, 825–840.
- Brody, D.L., and Yue, D.T. (2000). Release-independent short-term synaptic depression in cultured hippocampal neurons. *J. Neurosci.* **20**, 2480–2494.
- Bucurenciu, I., Kulik, A., Schwaller, B., Frotscher, M., and Jonas, P. (2008). Nanodomain coupling between Ca^{2+} channels and Ca^{2+} sensors promotes fast and efficient transmitter release at a cortical GABAergic synapse. *Neuron* **57**, 536–545.
- Catterall, W.A., and Few, A.P. (2008). Calcium channel regulation and presynaptic plasticity. *Neuron* **59**, 882–901.
- Debanne, D. (2004). Information processing in the axon. *Nat. Rev. Neurosci.* **5**, 304–316.
- Delaney, K.R., and Zucker, R.S. (1990). Calcium released by photolysis of DM-nitrophen stimulates transmitter release at squid giant synapse. *J. Physiol.* **426**, 473–498.
- Dittman, J.S., and Regehr, W.G. (1998). Calcium dependence and recovery kinetics of presynaptic depression at the climbing fiber to Purkinje cell synapse. *J. Neurosci.* **18**, 6147–6162.
- Engel, D., and Jonas, P. (2005). Presynaptic action potential amplification by voltage-gated Na^+ channels in hippocampal mossy fiber boutons. *Neuron* **45**, 405–417.
- Fernández-Alfonso, T., and Ryan, T.A. (2004). The kinetics of synaptic vesicle pool depletion at CNS synaptic terminals. *Neuron* **41**, 943–953.
- Fioravante, D., and Regehr, W.G. (2011). Short-term forms of presynaptic plasticity. *Curr. Opin. Neurobiol.* **21**, 269–274.
- Galarreta, M., and Hestrin, S. (1998). Frequency-dependent synaptic depression and the balance of excitation and inhibition in the neocortex. *Nat. Neurosci.* **1**, 587–594.
- Geiger, J.R., and Jonas, P. (2000). Dynamic control of presynaptic Ca^{2+} inflow by fast-inactivating K^+ channels in hippocampal mossy fiber boutons. *Neuron* **28**, 927–939.
- Hallermann, S., Pawlu, C., Jonas, P., and Heckmann, M. (2003). A large pool of releasable vesicles in a cortical glutamatergic synapse. *Proc. Natl. Acad. Sci. USA* **100**, 8975–8980.
- He, L., Wu, X.S., Mohan, R., and Wu, L.G. (2006). Two modes of fusion pore opening revealed by cell-attached recordings at a synapse. *Nature* **444**, 102–105.
- Hefft, S., Kraushaar, U., Geiger, J.R., and Jonas, P. (2002). Presynaptic short-term depression is maintained during regulation of transmitter release at a GABAergic synapse in rat hippocampus. *J. Physiol.* **539**, 201–208.
- Heidelberger, R., Heinemann, C., Neher, E., and Matthews, G. (1994). Calcium dependence of the rate of exocytosis in a synaptic terminal. *Nature* **371**, 513–515.
- Hirano, T., and Kasono, K. (1993). Spatial distribution of excitatory and inhibitory synapses on a Purkinje cell in a rat cerebellar culture. *J. Neurophysiol.* **70**, 1316–1325.
- Hu, H., and Jonas, P. (2014). A supercritical density of Na^+ channels ensures fast signaling in GABAergic interneuron axons. *Nat. Neurosci.* **17**, 686–693.
- Jonas, P., Bischofberger, J., Fricker, D., and Miles, R. (2004). Interneuron Diversity series: Fast in, fast out—temporal and spatial signal processing in hippocampal interneurons. *Trends Neurosci.* **27**, 30–40.
- Kaneko, M., Yamaguchi, K., Eiraku, M., Sato, M., Takata, N., Kiyohara, Y., Mishina, M., Hirase, H., Hashikawa, T., and Kengaku, M. (2011). Remodeling of monopolar Purkinje cell dendrites during cerebellar circuit formation. *PLoS ONE* **6**, e20108.
- Kawaguchi, S.Y., and Hirano, T. (2007). Sustained structural change of GABA_A receptor-associated protein underlies long-term potentiation at inhibitory synapses on a cerebellar Purkinje neuron. *J. Neurosci.* **27**, 6788–6799.
- Khalilq, Z.M., and Raman, I.M. (2005). Axonal propagation of simple and complex spikes in cerebellar Purkinje neurons. *J. Neurosci.* **25**, 454–463.
- Kirischuk, S., Clements, J.D., and Grantyn, R. (2002). Presynaptic and postsynaptic mechanisms underlie paired pulse depression at single GABAergic boutons in rat collicular cultures. *J. Physiol.* **543**, 99–116.
- Kraushaar, U., and Jonas, P. (2000). Efficacy and stability of quantal GABA release at a hippocampal interneuron-principal neuron synapse. *J. Neurosci.* **20**, 5594–5607.
- Kushmerick, C., Renden, R., and von Gersdorff, H. (2006). Physiological temperatures reduce the rate of vesicle pool depletion and short-term depression via an acceleration of vesicle recruitment. *J. Neurosci.* **26**, 1366–1377.
- Lawrence, J.J., and McBain, C.J. (2003). Interneuron diversity series: containing the detonation—feedforward inhibition in the CA3 hippocampus. *Trends Neurosci.* **26**, 631–640.
- Leão, R.M., Kushmerick, C., Pinaud, R., Renden, R., Li, G.L., Taschenberger, H., Spiro, G., Levinson, S.R., and von Gersdorff, H. (2005). Presynaptic Na^+ channels: locus, development, and recovery from inactivation at a high-fidelity synapse. *J. Neurosci.* **25**, 3724–3738.
- Lindgren, C.A., and Moore, J.W. (1989). Identification of ionic currents at presynaptic nerve endings of the lizard. *J. Physiol.* **414**, 201–222.
- Loewenstein, Y., Mahon, S., Chadderton, P., Kitamura, K., Sompolinsky, H., Yarom, Y., and Häusser, M. (2005). Bistability of cerebellar Purkinje cells modulated by sensory stimulation. *Nat. Neurosci.* **8**, 202–211.
- Mennerick, S., and Matthews, G. (1996). Ultrafast exocytosis elicited by calcium current in synaptic terminals of retinal bipolar neurons. *Neuron* **17**, 1241–1249.
- Millar, A.G., Zucker, R.S., Ellis-Davies, G.C., Charlton, M.P., and Atwood, H.L. (2005). Calcium sensitivity of neurotransmitter release differs at phasic and tonic synapses. *J. Neurosci.* **25**, 3113–3125.
- Monsivais, P., Clark, B.A., Roth, A., and Häusser, M. (2005). Determinants of action potential propagation in cerebellar Purkinje cell axons. *J. Neurosci.* **25**, 464–472.
- Moulder, K.L., and Mennerick, S. (2005). Reluctant vesicles contribute to the total readily releasable pool in glutamatergic hippocampal neurons. *J. Neurosci.* **25**, 3842–3850.
- Neher, E., and Marty, A. (1982). Discrete changes of cell membrane capacitance observed under conditions of enhanced secretion in bovine adrenal chromaffin cells. *Proc. Natl. Acad. Sci. USA* **79**, 6712–6716.
- Neher, E., and Sakaba, T. (2008). Multiple roles of calcium ions in the regulation of neurotransmitter release. *Neuron* **59**, 861–872.
- Novak, P., Gorelik, J., Vivekananda, U., Shevchuk, A.I., Ermolyuk, Y.S., Bailey, R.J., Bushby, A.J., Moss, G.W., Rusakov, D.A., Klenerman, D., et al. (2013). Nanoscale-targeted patch-clamp recordings of functional presynaptic ion channels. *Neuron* **79**, 1067–1077.
- Orduz, D., and Lliano, I. (2007). Recurrent axon collaterals underlie facilitating synapses between cerebellar Purkinje cells. *Proc. Natl. Acad. Sci. USA* **104**, 17831–17836.
- Palay, S.L., and Chan-Palay, V. (1974). *Cerebellar cortex: Cytology and organization.* (Springer).
- Pan, B., and Zucker, R.S. (2009). A general model of synaptic transmission and short-term plasticity. *Neuron* **62**, 539–554.
- Pedroarena, C.M., and Schwarz, C. (2003). Efficacy and short-term plasticity at GABAergic synapses between Purkinje and cerebellar nuclei neurons. *J. Neurophysiol.* **89**, 704–715.
- Prakriya, M., and Mennerick, S. (2000). Selective depression of low-release probability excitatory synapses by sodium channel blockers. *Neuron* **26**, 671–682.
- Pugh, J.R., and Raman, I.M. (2005). GABA_A receptor kinetics in the cerebellar nuclei: evidence for detection of transmitter from distant release sites. *Biophys. J.* **88**, 1740–1754.
- Pugh, J.R., and Raman, I.M. (2006). Potentiation of mossy fiber EPSCs in the cerebellar nuclei by NMDA receptor activation followed by postinhibitory rebound current. *Neuron* **51**, 113–123.

- Rancz, E.A., Ishikawa, T., Duguid, I., Chadderton, P., Mahon, S., and Häusser, M. (2007). High-fidelity transmission of sensory information by single cerebellar mossy fibre boutons. *Nature* *450*, 1245–1248.
- Sakaba, T. (2008). Two Ca^{2+} -dependent steps controlling synaptic vesicle fusion and replenishment at the cerebellar basket cell terminal. *Neuron* *57*, 406–419.
- Sakaba, T., and Neher, E. (2001). Calmodulin mediates rapid recruitment of fast-releasing synaptic vesicles at a calyx-type synapse. *Neuron* *32*, 1119–1131.
- Sankaranarayanan, S., and Ryan, T.A. (2001). Calcium accelerates endocytosis of vSNAREs at hippocampal synapses. *Nat. Neurosci.* *4*, 129–136.
- Saviane, C., and Silver, R.A. (2006). Fast vesicle reloading and a large pool sustain high bandwidth transmission at a central synapse. *Nature* *439*, 983–987.
- Schneggenburger, R., and Neher, E. (2000). Intracellular calcium dependence of transmitter release rates at a fast central synapse. *Nature* *406*, 889–893.
- Shin, M., Moghadam, S.H., Sekirnjak, C., Bagnall, M.W., Kolkman, K.E., Jacobs, R., Faulstich, M., and du Lac, S. (2011). Multiple types of cerebellar target neurons and their circuitry in the vestibulo-ocular reflex. *J. Neurosci.* *31*, 10776–10786.
- Smith, S.M., Bergsman, J.B., Harata, N.C., Scheller, R.H., and Tsien, R.W. (2004). Recordings from single neocortical nerve terminals reveal a nonselective cation channel activated by decreases in extracellular calcium. *Neuron* *41*, 243–256.
- Southan, A.P., and Robertson, B. (1998). Patch-clamp recordings from cerebellar basket cell bodies and their presynaptic terminals reveal an asymmetric distribution of voltage-gated potassium channels. *J. Neurosci.* *18*, 948–955.
- Stevens, C.F., and Wesseling, J.F. (1998). Activity-dependent modulation of the rate at which synaptic vesicles become available to undergo exocytosis. *Neuron* *21*, 415–424.
- Sun, J.Y., and Wu, L.G. (2001). Fast kinetics of exocytosis revealed by simultaneous measurements of presynaptic capacitance and postsynaptic currents at a central synapse. *Neuron* *30*, 171–182.
- Takei, K., Stukenbrok, H., Metcalf, A., Mignery, G.A., Südhof, T.C., Volpe, P., and De Camilli, P. (1992). Ca^{2+} stores in Purkinje neurons: endoplasmic reticulum subcompartments demonstrated by the heterogeneous distribution of the InsP3 receptor, Ca^{2+} -ATPase, and calsequestrin. *J. Neurosci.* *12*, 489–505.
- Taschenberger, H., and von Gersdorff, H. (2000). Fine-tuning an auditory synapse for speed and fidelity: developmental changes in presynaptic waveform, EPSC kinetics, and synaptic plasticity. *J. Neurosci.* *20*, 9162–9173.
- Telgkamp, P., and Raman, I.M. (2002). Depression of inhibitory synaptic transmission between Purkinje cells and neurons of the cerebellar nuclei. *J. Neurosci.* *22*, 8447–8457.
- Telgkamp, P., Padgett, D.E., Ledoux, V.A., Woolley, C.S., and Raman, I.M. (2004). Maintenance of high-frequency transmission at purkinje to cerebellar nuclear synapses by spillover from boutons with multiple release sites. *Neuron* *41*, 113–126.
- Vincent, P., and Marty, A. (1996). Fluctuations of postsynaptic inhibitory postsynaptic currents from rat cerebellar slices. *J. Physiol.* *494*, 183–196.
- Volynski, K.E., Rusakov, D.A., and Kullmann, D.M. (2006). Presynaptic fluctuations and release-independent depression. *Nat. Neurosci.* *9*, 1091–1093.
- von Gersdorff, H., and Matthews, G. (1994). Dynamics of synaptic vesicle fusion and membrane retrieval in synaptic terminals. *Nature* *367*, 735–739.
- Wu, X.S., Sun, J.Y., Evers, A.S., Crowder, M., and Wu, L.G. (2004). Isoflurane inhibits transmitter release and the presynaptic action potential. *Anesthesiology* *100*, 663–670.
- Xu, J., and Wu, L.G. (2005). The decrease in the presynaptic calcium current is a major cause of short-term depression at a calyx-type synapse. *Neuron* *46*, 633–645.
- Zucker, R.S., and Regehr, W.G. (2002). Short-term synaptic plasticity. *Annu. Rev. Physiol.* *64*, 355–405.

Neuron, Volume 85

Supplemental Information

Control of Inhibitory Synaptic Outputs

by Low Excitability of Axon Terminals

Revealed by Direct Recording

Shin-ya Kawaguchi and Takeshi Sakaba

Inventory of Supplemental Information

·Supplemental Figures

Figure S1	-----	related to Figure 1
Figure S2	-----	related to Figure 3
Figure S3	-----	related to Figure 4
Figure S4	-----	related to Figure 6
Figure S5	-----	related to Figure 7
Figure S6	-----	related to Figure 8

·Supplemental Experimental Procedures

·Supplemental References

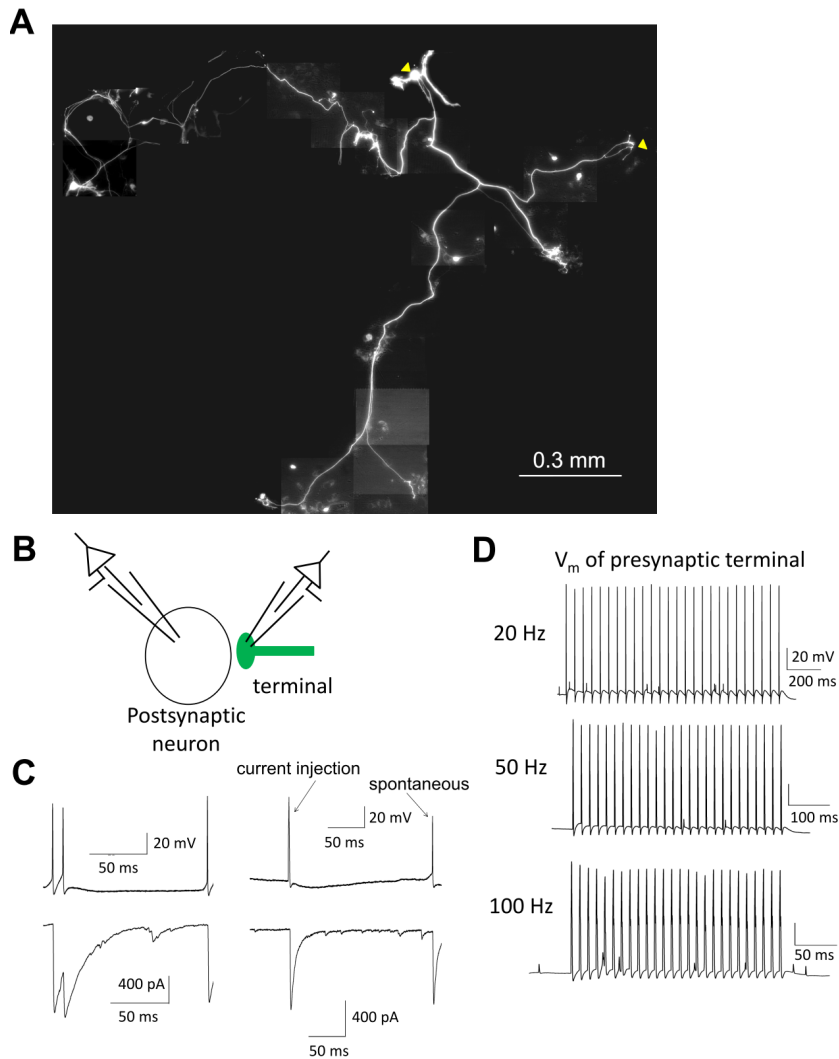


Figure S1, related to Figure 1. Stimulation of current-clamped presynaptic terminal

A, Fluorescent images of an EGFP-labeled cultured PC. The soma and an axon terminal shown in Fig. 1 are highlighted by yellow arrowheads. **B**, A scheme of paired recordings from a presynaptic PC axon terminal and the target neuron. **C**, Left: Spontaneous presynaptic action potential firing and the evoked IPSC, showing paired pulse depression. Right: Rapid and large current injection (1 ms, 800 pA) to the presynaptic terminal caused action potential-like discharge of membrane potential, causing IPSC with similar amplitude and time course to the IPSC upon spontaneous presynaptic action potential. As shown in Fig. S4, sustained current injection with smaller amplitude (200 pA, 10 msec) to the terminal often failed to trigger action potentials. **D**, Action potential-like depolarization in a presynaptic terminal caused by direct current injection to the terminal at 20, 50, and 100 Hz.

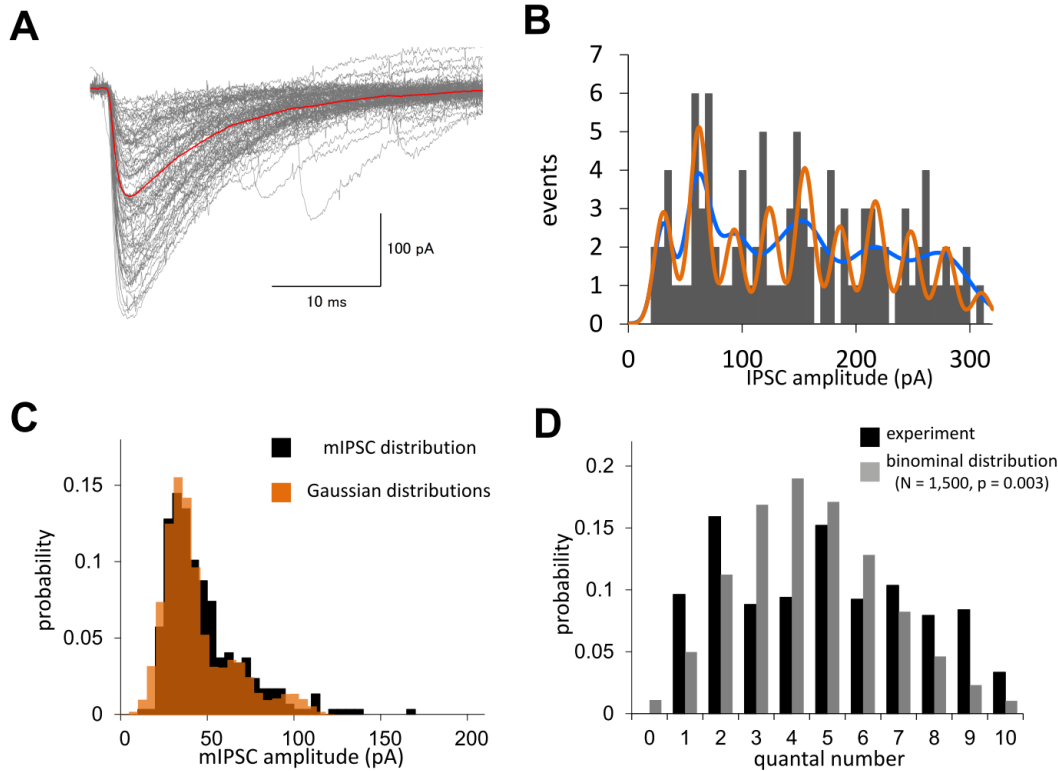


Figure S2, related to Figure 3.

Quantal analysis of single synaptic IPSCs caused by terminal stimulation.

A, Mean IPSC (red) was obtained by averaging 83 IPSC traces with discrete steps (gray). **B**, IPSC amplitude distribution histogram with apparently 10 discrete steps recorded from a pair of PC terminal and postsynaptic neuron. Orange and blue curves show fitting of the IPSC distribution with combinations of single Gaussian distribution defined by mean and standard deviation of 31 and 9 pA, respectively. The fit is better when we assume equal variance for each peak (orange) rather than increasing variance with larger peaks (blue), which may indicate that the number of postsynaptic receptors is limited for each release site (Auger and Marty, 2000; Edwards et al., 1990). **C**, Distribution of mIPSC (~ 289) amplitudes (black) and combinations of Gaussian distributions of quantal IPSC (orange) estimated from B. Two peaks might be due to multivesicular release which is seen under resting condition at GABAergic synapses (Kraushaar and Jonas, 2000; Llano and Gerschenfeld, 1993). **D**, Distribution of quantal number in a single synapse estimated by the experimental data. Similar recordings have been obtained from 6 pairs. For comparison, we also show a binomial distribution assuming total release-ready sites ($N = 1,500$) and release probability ($Pr = 0.003$), which were estimated from the Cm measurements and from the ratio of the mean evoked-IPSC amplitude and the mean mIPSC amplitude.

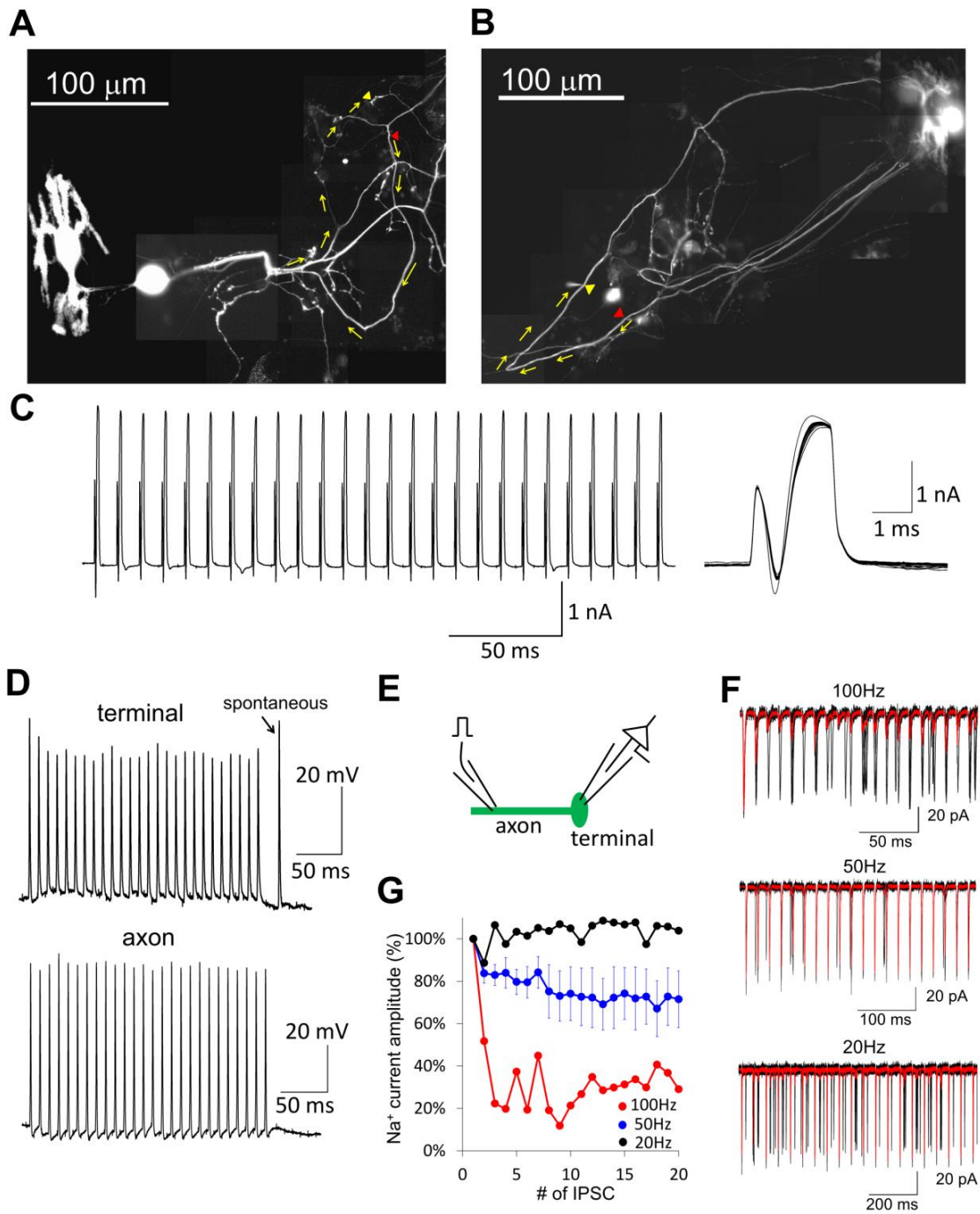


Figure S3, related to Figure 4. Attenuation of action potential trains at terminals.

A, B, Whole images of a PC axon paired-recorded at two distinct axonal sites or at an axon and its terminal. Lower magnified images of a PC axon and a terminal shown in Fig. 4A (**A**) or two sites of an axon shown in Fig. 4D (**B**). Action potentials were evoked at the site of an axon

(indicated by red arrowheads), conducting as indicated by yellow arrows, and recorded from the terminal (**A**) or from the axon (**B**) as indicated by yellow arrowheads. Where axons were crossing, we distinguished them by changing focus. **C**, Representative trace of sodium currents at 100 Hz train stimulation recorded from the stimulation electrode at the axon. Although sodium currents were securely elicited by 2-ms depolarization pulse (0 mV) with slight modulation in the amplitude, action potential failed to conduct to the terminal as shown in 'example 1' of Fig. 4B. **D**, Instead of depolarization pulses, current injection (at 100 Hz) was used to trigger action potentials train at a site of an axon, and the conducting action potentials were recorded at the terminal (top) or at another site of the axon (bottom). Action potentials triggered by current injection also showed attenuation around the axon terminal, but not in the axon. **E**, Experimental scheme of terminal-recording of sodium currents propagating along an axon to the terminal from the site where extracellular electrical stimulation was applied. This set of experiments was carried out to preserve intact axons. See F and G for results. **F**, Representative traces of sodium current trains at 20, 50, and 100Hz recorded from a terminal. For each, 10 individual traces (black) are superimposed together with an averaged trace (red). **G**, Normalized amplitudes (mean \pm SEM) of action sodium currents to the first one. N = 1 cell for 100Hz, 4 for 50 Hz, and 1 for 20 Hz.

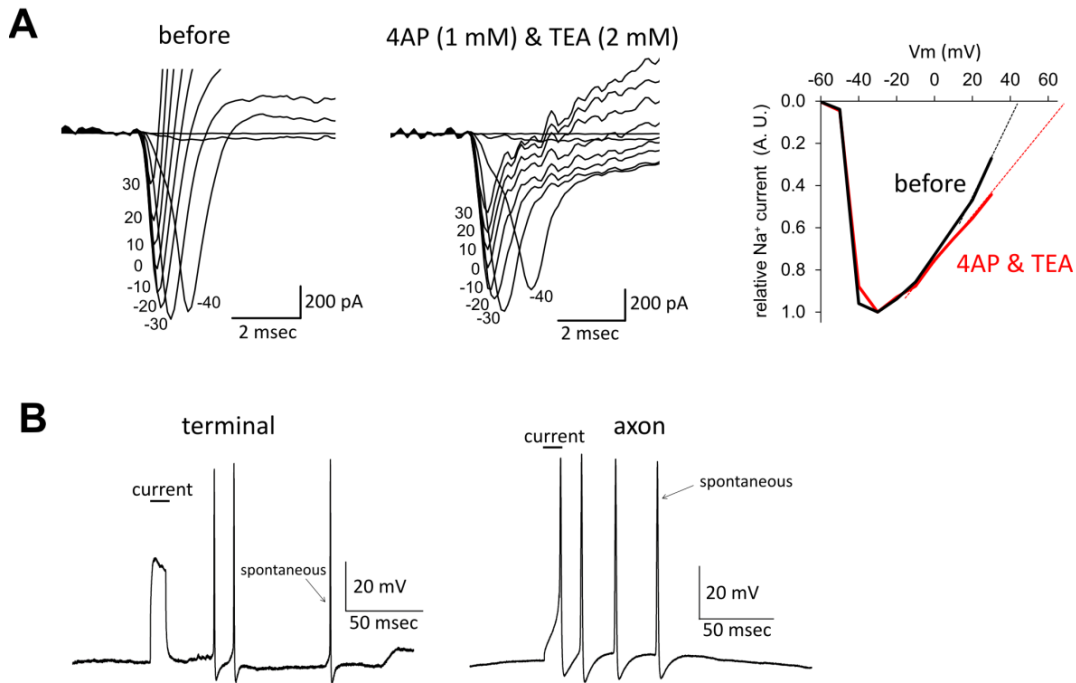


Figure S4, related to Figure 6. Low membrane excitability at axon terminals.

A, Representative sodium currents recorded from an axon terminal before (left) and after (middle) inhibition of K⁺ channels by 4AP (1 mM) and TEA (2 mM). I-V curves obtained in the absence and presence of K⁺ channels blockers (right) suggest that Na⁺ current amplitudes at positive V_m (> 20 mV) are apparently smaller because of contamination of K⁺ conductance. **B**, Representative membrane potential changes upon current injection to an axon (right) and to a terminal (left). Current injection to the terminal was more difficult to trigger an AP firing compared to the axon when the same current injection (200 pA for 10 msec) was applied.

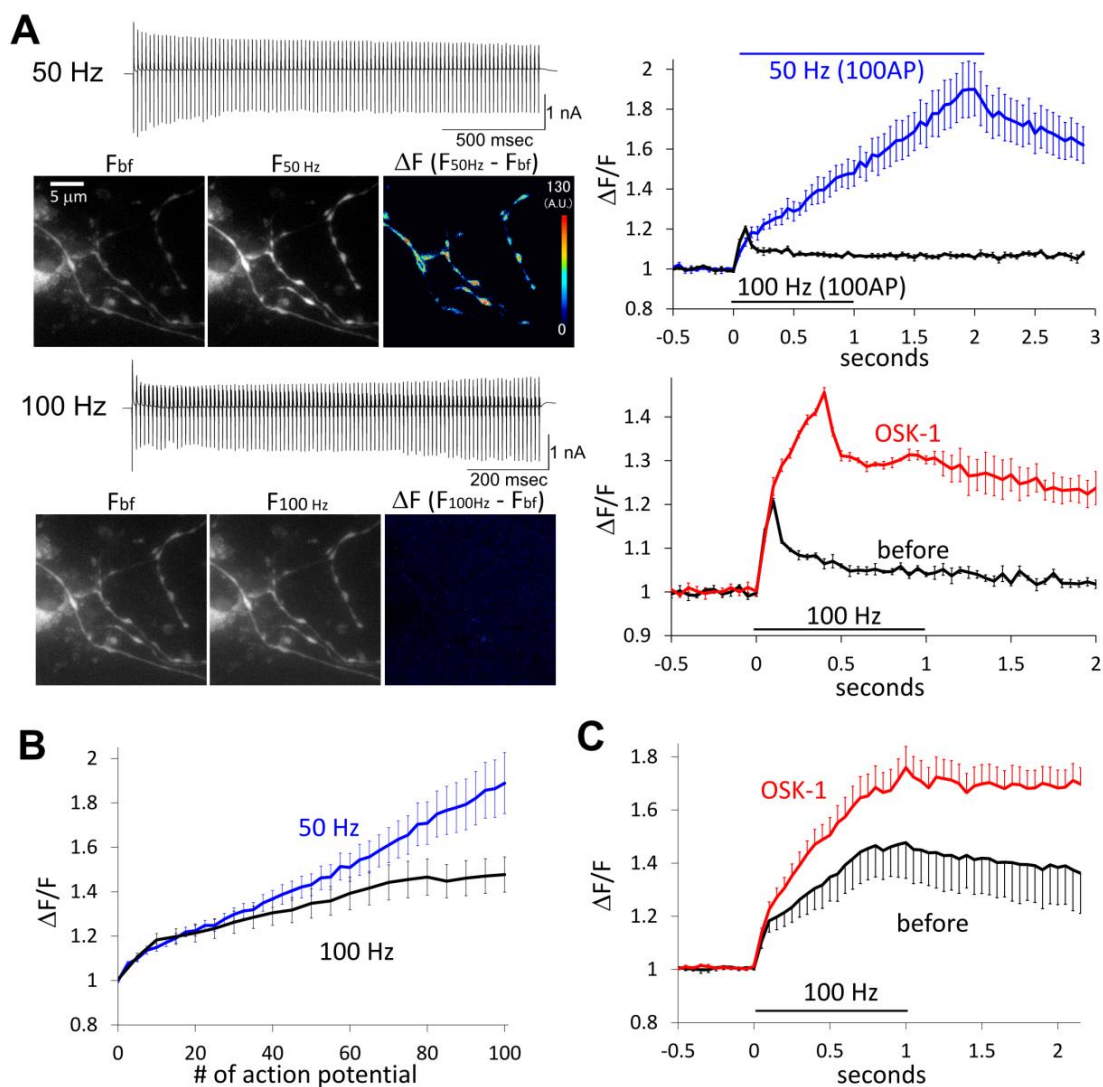


Figure S5, related to Figure 7. Ca^{2+} imaging of action potential attenuation.

A, Left, Representative sodium currents (100 pulses of 0 mV for 2 ms at 50 or 100 Hz) recorded from a PC soma and fluorescence images of OGB-1 (500 μM , applied through a somatic patch pipette) around axon terminals before (F_{bf}) and during ($F_{50\text{ Hz}}$ or $F_{100\text{ Hz}}$) the stimulation trains. Difference of fluorescence intensity before and during the stimulation (ΔF) is shown in pseudo-color. Right top, Time courses of relative ΔF at 50 or 100 Hz (in 5 terminals of 1 cell shown in left panels). In this example, Ca^{2+} level decreased during the 100 Hz stimulation whereas somatic sodium currents during the train were relatively constant (left). Thus, the data

are consistent with the idea that action potentials fail to conduct around the terminals. Right bottom, the Ca^{2+} increase at 100 Hz stimulation was augmented by OSK-1 application (20 nM).

B, Relative ΔF at 50 or 100 Hz (in 25 terminals from 5 cells) is plotted against the number of action potentials. Note that 100 Hz was less effective. **C**, Averaged time courses of relative ΔF of OGB-1 before and after OSK-1 application (20 nM). $n = 25$ terminals from 5 cells. Error bars represent SEM.

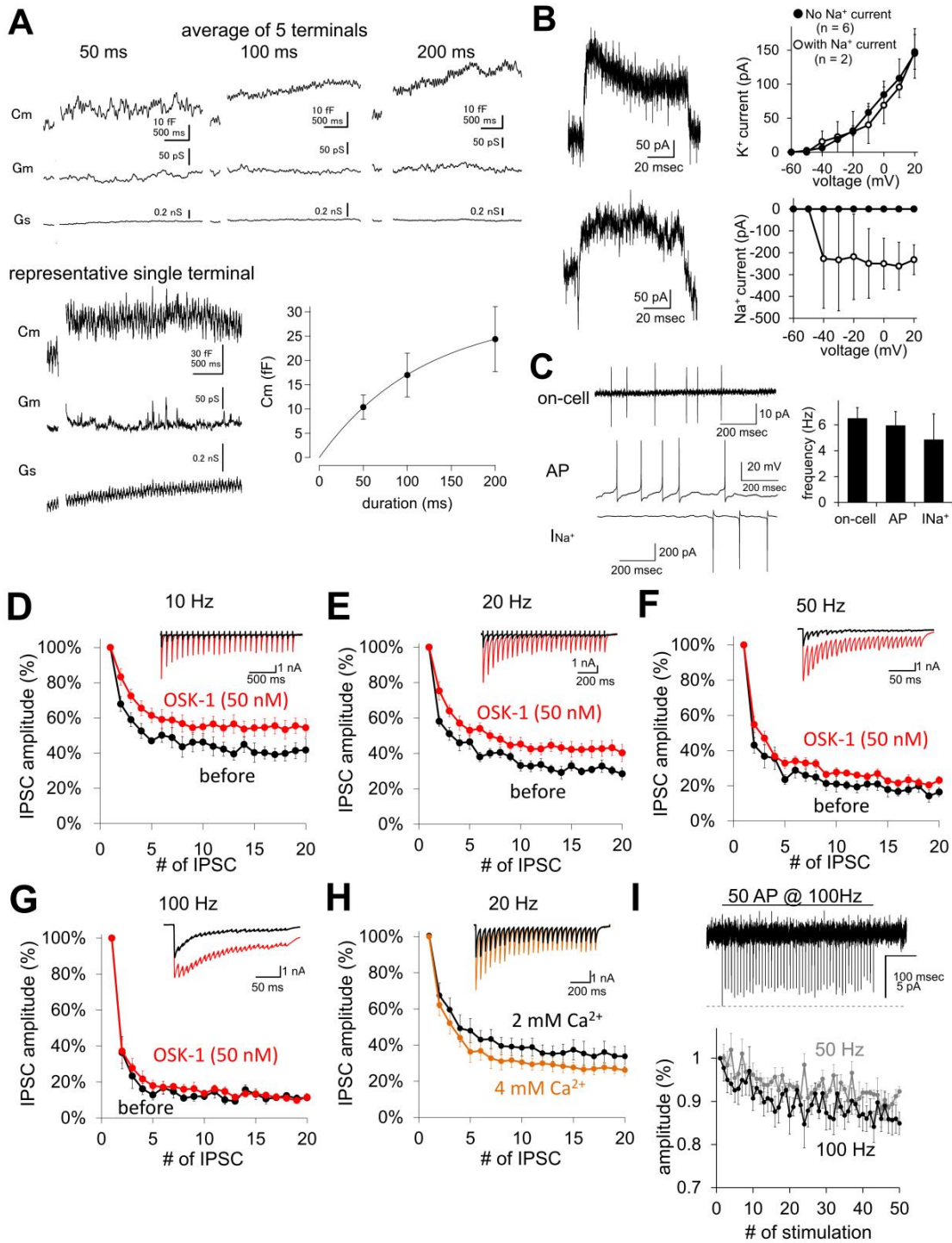


Figure S6, related to Figure 8.

Confirmation of low excitability of PC axon terminals in a slice.

A, Top panel: Average C_m increases caused by direct depolarization (0 mV for 50, 100, or 200

ms) of a PC axon terminal in the slice preparation (average of $n = 5$ terminals). There was no correlation to G_m and G_s . Therefore, capacitance changes most likely reflect synaptic vesicle exocytosis and endocytosis, confirming that the recording site is an axon terminal. Note that the time course of endocytosis is variable among cells in both culture and slices (see, Renden and von Gersdorff, 2007). Bottom left: Left shows example traces of C_m , G_m and G_s in response to a 100 ms pulse. Bottom right panel shows the capacitance jumps plotted against the pulse duration. The RRP size estimated from a single exponential fit was estimated to be 20-30 fF, and the time course of release was slower compared to the culture condition, indicating low Pr. Compared with the C_m jump recorded in cultured PC terminals, the C_m increase was smaller in slice on average, perhaps due to the immature stage at the time of experiments (P9-16 for slice recordings vs DIV 30-45 for culture recordings, Taschenberger et al., 2002 for developmental increase in the pool size). Nevertheless, the vesicle pool is variable in culture (30-250 fF), and the value may be within the range of variability. The RRP size is still large in slices, consisting of 300-600 vesicles on average. **B**, Na^+ and K^+ currents recorded from a PC axon terminal in slice. In only 2 out of 8 cells, Na^+ current could be detected. It was hard to elicit action potentials using current injection, consistent with low excitability of the terminal. **C**, Representative traces of action potentials recorded from an axon terminal of cultured PC in on-cell, current-clamp, and voltage-clamp modes. Mean firing frequencies of a PC detected by each recording mode from 4 cells. **D-G**, K^+ channel blockade-mediated inhibition of IPSC depression at PC-DCN synapses in a cerebellar slice. Representative traces (average of 10 traces) and normalized amplitudes of IPSC trains at 10 (D), 20 (E), 50 (F), and 100 Hz (G) before (black) and after (red) OSK-1 (50 nM) application. IPSCs were triggered by stimulation of axon bundles in white matter. $N = 8$ cells. Compared with data shown in Fig. 8, the depression in each condition was stronger in control condition, and the effect of OSK-1 to suppress depression shifted to somewhat lower frequency. This might be due to the cooperative working of several depression

mechanisms at PC synapses on a DCN neuron, such as transmitter pooling, postsynaptic receptor desensitization (Telgkamp et al., 2004), and action potential attenuation. The potent postsynaptic GABA_A receptor desensitization occurring slowly even with low frequency stimulation (Pugh and Raman, 2005) might have masked the OSK-1 sensitive depression component particularly at high frequency (~ 100 Hz), especially when Pr per synapse (not per release site) was high and receptors were exposed to high concentration of GABA. **H**, Representative traces (average of 10 traces) and normalized amplitudes of IPSC trains at 20 Hz in the presence of 2 (black) and 4 mM Ca²⁺ (orange) in the external solution. n = 4 cells. Although raising external Ca²⁺ augmented IPSC amplitudes similarly to OSK-1, the frequency-dependent depression was not weakened and rather got deeper. **I**, Representative trace (top panel, averaged from 20 traces) and changes in spike amplitudes during an action-potential train (100 Hz and 50 Hz, bottom panel) extracellularly recorded from a cerebellar basket cell (BC) axon terminal at physiological temperature (n = 7 cells for 100Hz, n = 5 cells for 50 Hz). Extracellular spikes are complex signals arising from the either first derivative of the action potentials along with a signal that is dictated by Na⁺ and K⁺ currents during the action potential. Nevertheless, their amplitude should reflect the intracellular action potential amplitudes (Henze et al., 2000). Spike attenuation was seen at the BC terminal, and because transmitter release is supra-linearly dependent on the Ca²⁺ (3rd power, Sakaba, 2008), attenuation of the spikes (sometimes larger than average because of fluctuation by trial to trial) should have a large impact on the IPSC amplitudes. Similar results have been obtained at room temperature. In order to verify the spike recordings, we also looked at Ca²⁺ dynamics in the terminal at room temperature, and have seen a sub-linear increase during a 50 Hz or 100 Hz stimulation, consistent with less Ca²⁺ influx during the train stimulation (n = 3, data not shown). Therefore, it is likely that action potential amplitudes were attenuated at the BC terminal. Data are presented as mean ± SEM.

Supplemental Experimental Procedures

Animal usage

For preparing dissociated culture and acute slice from cerebellum, Wistar rats (P0 for dissociated culture, and P9-21 for slice) were decapitated in accordance with the guidelines regarding care and use of animals for experimental procedures of the National Institutes of Health, U.S.A. and Doshisha University, which was approved by the local committee for handling experimental animals in Doshisha University.

Culture

The method for preparing primary cultures of cerebellar neurons was similar to that in a previous study (Kawaguchi and Hirano, 2007). PCs were transfected with EGFP at 7 days after culture with adeno-associated virus (AAV) vector carrying EGFP under the control of CAG promoter (AAV-CAG-EGFP) (Kaneko et al., 2011). PCs could be visually identified by their large cell bodies and thick dendrites, and EGFP fluorescence which preferentially labeled PCs by relatively specific AAV infection. An axon of PC was clearly different from dendrites which have high density of spines, and the preferential localization of Na⁺ channels in an axon accorded to the morphological discrimination. The postsynaptic neurons targeted by PCs had three features, which led us to conclude that they were DCN neurons. (1) The neurons had a relatively large cell body of > 12 μm (usually DCN neurons are large). (2) Some neurons were positive for SMI-32 monoclonal antibody (a marker for DCN glutamatergic

neurons and PCs). (3) The neurons exhibited hyperpolarization-induced inward currents and rebound depolarization, characteristics of DCN neurons (data not shown). We should also note that the neurons innervated by PCs are apparently different from GABAergic interneurons such as stellate and basket neurons which have thin cell bodies, and were negative for neurogranin staining (a Golgi cell marker) (data not shown). PCs and granule cells have clearly different morphology. Whole-cell patch clamp recordings, fluorescent imaging, and immunocytochemistry were performed 4-6 weeks after preparation of the culture. Hippocampal neurons were cultured in Neurobasal medium (Gibco) with B27 supplement (Gibco), and used for patch clamp recordings 10-16 days after the culture.

Slice preparation

Rat sagittal brain slices (200-300 μm , P9-P16 for PC-DCN, P14-21 for BC-PC) of cerebellar vermis were prepared with a Leica VT1200S slicer in the ice-cold solution containing the following (in mM): 60 NaCl, 120 sucrose, 25 NaHCO₃, 1.25 NaH₂PO₄, 2.5 KCl, 25 D-glucose, 0.4 ascorbic acid, 3 myo-inositol, 2 Na-pyruvate, 0.1 CaCl₂, and 3MgCl₂. Slices were incubated at 37 °C for 1 h in a saline containing the following (in mM): 125 NaCl, 2.5 KCl, 25 NaHCO₃, 1.25 NaH₂PO₄, 25 D-glucose, 0.4 ascorbic acid, 3 myo-inositol, 2 Na-pyruvate, 2 CaCl₂, and 1 MgCl₂.

DNA construction and transfection

CAG promoter-based AAV vector for EGFP transfection was a generous gift from Dr.

Kengaku (Kyoto Univ.). cDNAs of sypHy (synaptophysin-pHluorin) and synapto-pHluorin (synaptobrevin-pHluorin) were obtained from Addgene (plasmid #24478) and from Dr. Tomoo Hirano (Kyoto Univ.), and were inserted into pCAGplay expression vector (Kawaguchi & Hirano, 2006) or into pAAV-CA-MCS (Kaneko et al., 2011). Both pHluorin-fused probes were transfected by direct microinjection of cDNA into the nucleus of a PC through a sharp glass pipette or by AAV infection.

Electrophysiology

Methods used for electrophysiological experiments were similar to those in previous studies (Kawaguchi and Hirano, 2007; Sakaba, 2008). Whole-cell patch clamp recording from a cultured PC was performed with an amplifier (EPC7 or EPC10, HEKA, Germany) at room temperature (20~24 °C) or at physiological temperature (32~36 °C), in a solution containing (in mM) 145 NaCl, 5 KOH, 2 CaCl₂, 1 MgCl₂, 10 Hepes, and 10 glucose (pH 7.3). In some experiments, 2,3-Dioxo-6-nitro-1,2,3,4-tetrahydrobenzo[f]quinoxaline-7-sulfonamide (NBQX, 10 μM, Tocris Cookson, UK), and tetrodotoxin (TTX, 1 μM, Wako, Japan) were used to inhibit glutamatergic EPSCs, APs, respectively. To inhibit K⁺ channels, TEA (2 or 10 mM), OSK-1 (10-100 nM, Alomone Lab), Dendrotoxin K (50 nM, Alomone Lab), Margatoxin (500 nM, Alomone Lab), or Agitoxin (750 nM, Alomone Lab) was applied to the bath. A patch pipette used to record from the soma, axon, and the terminal of a PC was filled with an internal solution (pH 7.3, adjusted by CsOH or KOH) containing (in mM) 155 CsCl, 0.5 ethylene glycol bis (β-aminoethylether) N,N,N',N'-tetraacetic acid (EGTA), 10 Hepes, 2 Mg-ATP and 0.2

Na-GTP, or that containing 155 KCl, 0.5 EGTA, 10 Hepes, 2 Mg-ATP and 0.2 Na-GTP. The Cs solution was used for measuring Ca^{2+} currents and presynaptic capacitance, and TTX and TEA were added extracellularly. Also for recording of IPSCs at the PC target neurons, the Cs-based solution was used. The K^+ internal solution was used to measure membrane excitability in current clamp and to measure Na^+ and K^+ currents at the PC soma, terminal or axon. The membrane potential of a PC was held at -70 mV except for capacitance measurements. Postsynaptic neurons were voltage clamped at -50 to -100 mV during IPSC recordings to avoid contamination of Na^+ currents. Series resistance of the PC soma, axon and axon terminal was, $18 \pm 1 \text{ M}\Omega$ ($n = 5$ cells), $62 \pm 8 \text{ M}\Omega$ ($n = 19$ cells), and $64 \pm 4 \text{ M}\Omega$ ($n = 48$ cells), respectively. Series resistance of the terminal was corrected by 40-90 %. On-line series resistance compensation (40 - 80 %) was applied to postsynaptic DCN neuron (usually 15-30 $\text{M}\Omega$), and the remaining resistance was corrected off-line after the recording. To evoke synaptic transmission, the PC soma or axon terminal was stimulated by depolarization pulses to 0-20 mV for 2-5 ms (soma and terminal) or by current injection of 0.5-1 nA for 1-2 ms (terminal). TeNT (100 nM, List Biological Lab) was applied into the terminal through a patch pipette in some experiments.

For recording from a DCN neuron or a PC as a postsynaptic neuron in slice preparation, the following internal solution was used (in mM): 170 CsCl, 2 EGTA, 10 Hepes, 0.5 QX314, 2 Mg-ATP and 0.2 Na-GTP. For presynaptic recordings of PC or BC, we used K^+ -based internal solution containing (in mM): 140 KGluconate, 20-30 KCl, 0.1-0.5 EGTA, 10 Hepes, 5 Mg-ATP, 4 Na Phosphocreatine and 0.5 Na-GTP. For recording IPSCs from the DCN neuron, white matter was stimulated briefly (10-50 V

for 0.1-0.2ms) using a glass pipette. Paired recordings from a BC and a PC have been described in Sakaba (2008), except that the experiments were done in physiological temperature (32-36°C). In some experiments, NBQX (10 μ M) was added extracellularly. Usually the membrane potential was held at -70 mV.

In order to visualize a PC axon in the DCN, DiO (0.5 % in Ringer solution) was applied locally through a glass pipette placed on the white matter of sagittal cerebellar slice. By waiting for 30 minutes, axons were visualized. For recording extracellular spikes, a small patch pipette (15-20 M Ω) filled with Ringer solution was used. Spikes were reliably recorded when resistance was more than 30-50 M Ω under voltage clamp mode at 0 mV. For patch clamp recordings we used a small patch pipette (15-20 M Ω) containing K⁺-based internal solution, which resulted in series resistance of 50-150 M Ω and capacitance of 0.5-2 pF. For recording spikes from the BC terminal, CF488 (100 μ M, Biotium) was added to K⁺ based internal solution and was included into the somatic patch pipette. After whole-cell dialysis for 10 minutes, the terminal region wrapping onto the PC was visualized. A small patch pipette filled with Ringer solution (15-20 M Ω) was approached to the terminal. Care was taken not to damage the terminal. We did not measure from en-passant type terminals in this study.

Capacitance measurements were carried out using sine + DC technique (Neher and Marty, 1982; Lindau and Neher, 1988) implemented on the Patchmaster software (HEKA, Germany). Presynaptic terminals were held at -80 mV and the sine wave (1000 or 2000 Hz and the peak amplitude of 30 mV) were applied on the holding potential. Sine wave of 1000 and 2000 Hz gave essentially the same results.

Because of large conductance changes during the depolarizing pulse, capacitance was usually measured between 200-300 msec after the pulse.

In order to examine the effective space clamp at the PC terminal in culture, we applied a small depolarizing or hyperpolarizing pulse (10 mV) to an axon or an axon terminal. Capacitive transients in response to the pulse should indicate the clamp area. Capacitive transients at an axon terminal followed a dual exponential with time constants of 0.13 ± 0.01 ms and 1.3 ± 0.2 ms ($n = 11$ cells). Assuming that the terminal was connected to a cylinder shape of axon, the terminal size was estimated to be 1.1 ± 0.1 pF, and a clamped axonal region had 1.8 ± 0.5 pF of capacitance. These membrane capacitances corresponded to a terminal with 3 μm diameter and an axon of 12 μm lengths inter-connected through a resistance of about 300 M Ω . Estimation of the efficiency of sine wave voltage change traveling to the axon outside the terminal by simulation suggested that it was hard to measure capacitance changes out of the recording terminal. Capacitive transients at the axon followed a dual exponential with a time constant of 0.25 ± 0.03 ms and 4.0 ± 1.0 ms ($n = 6$ cells), suggesting that axonal membrane is not homogenous probably due to wrapping by glial cells. Assuming a diameter of 1.5 μm , the effective length of an axon under relatively good clamp is 40 μm . Although Na^+ and K^+ current amplitudes could not be compared between an axon and a terminal because of different clamped areas, the ratio of Na^+ current amplitudes over K^+ current amplitudes should be informative for relative excitability.

The deconvolution analysis was used to estimate the time course of transmitter release (Van der Kloot, 1988; Diamond and Jahr, 1995; Neher and Sakaba, 2001). The IPSCs were deconvolved at 300

msec after the stimulation (the same timing to the C_m measurement) with the mIPSC waveform measured at the same cell. The mIPSC was similar in amplitude and time course to asynchronous release events observed during large Ca^{2+} influx to the terminal. Because the IPSC decay was relatively slow, the estimated release rates were not sensitive to the exact time course of mIPSCs (Neher and Sakaba, 2001). For analysis, we assumed that the IPSCs were a linear summation of mIPSCs.

Ca^{2+} uncaging in the PC terminal was performed by adding DM-nitrophen (2-5 mM, Calbiochem) and Fura2-FF (200 μ M, TEFLabs) to the internal solution containing (in mM) 130 CsCl, 20 HEPES, 5 Na-ATP, 0.5 MgCl₂, 1 Na-GTP, 1.8-4 CaCl₂ through a patch pipette. A UV flash lamp (illumination duration \sim 1 ms; Rapp, Germany) was used for photolysis of DM-nitrophen (Sakaba, 2008). $[Ca^{2+}]_i$ was monitored by alternative excitation of Fura-2FF at 350/380 nm with a monochromator (Polychrome 5, Till Photonics, Germany), and the images were captured with a CCD camera (VGA, Till Photonics). Fura-2FF fluorescence ratio (F350/F380) was calibrated in vitro ($R_{min} = 0.32$, R_{int} (for 10 μ M Ca^{2+}) = 1.07, and $R_{max} = 6.05$). Images of pHluorin fluorescence in PC axon terminals were obtained with Zyla sCMOS camera (Andor), and analyzed with SOLIS (Andor) or Image J (NIH).

Immunocytochemistry

Cultured neurons were fixed with 4 % paraformaldehyde in phosphate buffered saline, permeabilized with 0.5 % Tween 20, then blocked with 2 % horse serum, and finally labeled with primary and secondary antibodies. The following antibodies were used: rabbit polyclonal antibody

(pAb) against Kv1.1 (1 : 100, Alomone Lab, Israel), Kv1.3 (1 : 100, Alomone Lab, Israel), mouse monoclonal antibody (mAb) against Na⁺ channels (1 : 1000, Sigma), chick pAb against GFP (1 : 1000, Chemicon), rat mAb against GFP (1 : 1000, Nacalai Tesque, Japan), rabbit pAb against vesicular GABA transporter (VGAT, 1:1000, Synaptic Systems), and Alexa 488 or 568-conjugated pAbs against rabbit, mouse, rat or chick IgG (1:400, Molecular Probes). The fluorescence images were obtained with Zyla sCMOS camera (Andor), and analyzed with Image J software (NIH).

Statistics

Data are presented as mean \pm SEM. Statistical significance was assessed by paired t-test, unpaired Students' t-test, Mann-Whitney U test or ANOVA.

Supplemental References

- Diamond, J.S., and Jahr, C.E. (1995). Asynchronous release of synaptic vesicles determines the time course of AMPA receptor-mediated EPSCs. *Neuron* 15, 1097-1107.
- Edwards, F.A., Konnerth, A., and Sakmann, B. (1990). Quantal analysis of inhibitory synaptic transmission in the dentate gyrus of rat hippocampal slices: a patch-clamp study. *J. Physiol.* 430, 213-249.
- Henze, D.A., Borhegyi, Z., Csicsvari, J., Mamiya, A., Harris, K.D. and Buzsaki, G. (2000). Intracellular features predicted by extracellular recordings in vivo. *J. Neurophysiol.* 84, 390-400.
- Kawaguchi, S. and Hirano, T. (2006). Integrin $\alpha 3\beta 1$ suppresses long-term potentiation at inhibitory synapses on the cerebellar Purkinje neuron. *Mol. Cell. Neurosci.* 31, 416-426.
- Neher, E. and Sakaba, T. (2001). Combining deconvolution and noise analysis for the estimation of transmitter release rates at the calyx of held. *J. Neurosci.* 21, 444-461.
- Lindau, M. and Neher, E. (1988). Patch-clamp techniques for time-resolved capacitance measurements in single cells. *Pflugers Arch.* 411, 137-146.
- Llano, I., Gerscheffeld, H.M. (1993). Inhibitory synaptic currents in stellate cells of rat cerebellar slices. *J. Physiol.*, 468, 177-200.
- Renden, R. and von Gersdorff, H. (2007). Synaptic vesicle endocytosis at a CNS nerve terminal: faster kinetics at physiological temperatures and increased endocytotic capacity during maturation. *J. Neurophysiol.* 98, 3349-3359.
- Taschenberger, H., Leao, R.M., Rowland, K.C., Spirou, G. and von Gersdorff, H. (2002). Optimizing synaptic architecture and efficiency for high-frequency transmission. *Neuron* 36, 1127-1143.
- Van der Kloot, W. (1988). The kinetics of quantal release during end-plate currents at the frog neuromuscular junction. *J. Physiol.* 402, 605-626.